DESIGN WAVE AND WATER LEVELS FOR THE KAPITI COAST

Prepared for Kapiti District Council

March 2007

Suite 3, 17 Nobs Line, New Plymouth, New Zealand
T: 64-6-7585035 E: enquires@metocean.co.nz

Report Status

Version	Date	Status	Approved By:
RevA	08/03/2007	Draft for review	McComb
RevO	02/07/2007	Approved for release	McComb

It is the responsibility of the reader to verify the currency of the version number of this report. This report has been prepared by D. Johnson, D. Goring, P. McComb, B. Beamsley and R. Zynfogel

TABLE OF CONTENTS

LIST OF FIGURES

LIST OF TABLES

1 INTRODUCTION

For coastal planning purposes, the Kapiti District Council requires a definition of the wave and water level conditions along the coastline within its authority (Fig. 1.1). The scope of this work to provide:

- The ambient wave conditions along the coast;
- The extreme wave conditions along the coast for 1, 10, 50 and 100-year return periods;
- The design mean water levels due to tides, and
- The design mean water levels from storm surge and other low-frequency forcing.

MetOcean Solutions Ltd has been commissioned to undertake this scope of work. MSL have subcontracted Dr Derek Goring of Mulgor Consulting Ltd to provide specialised analysis and interpretation to define the water level component of the scope.

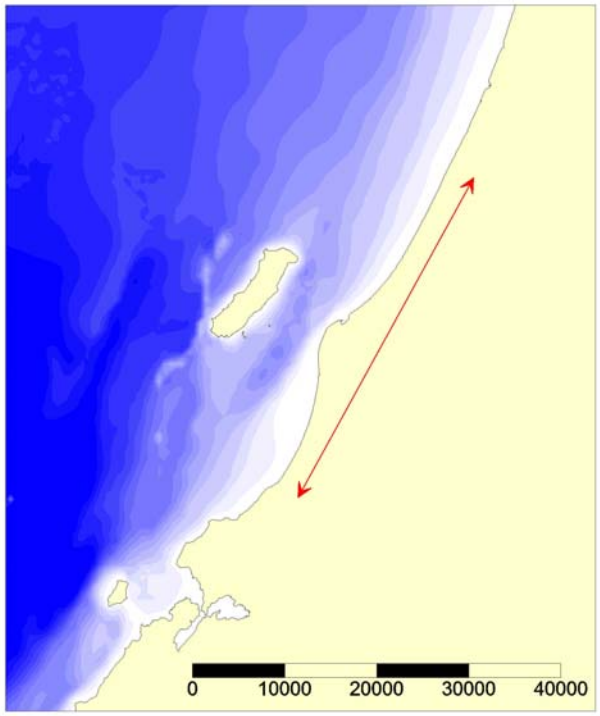

Figure 1.1 The study location between Paekakariki and Otaki

1.1 Report structure

The numerical hindcast modelling methods are detailed in Section 2 of this report, and the data sources for the water level analysis are described in Section 3. The analytical methods employed in this study are presented in Section 4. Results for the wave climate are provided in Section 5, and the water level results are included in Section 6. The results are summarised in Section 7 and the references cited in this report are listed in the final section.

Joint probability distribution tables of the wave height, wave period, and wave direction are appended to this report in an electronic format:

[KDC wave joint probability data MSL_March_2007.xls].

2 DATA SOURCES - WAVE HINDCAST MODELLING

2.1 Numerical model

SWAN (Simulating Waves Nearshore) was used for all of the wave modelling. SWAN is a third generation ocean wave propagation model, which solves the spectral action density balance equation for wavenumber-direction spectra. This means that the growth, refraction, and decay of each component of the complete sea state, each with a specific frequency and direction, is solved, giving a complete and realistic description of the wave field as it changes in time and space. Physical processes that are simulated include the generation of waves by the surface wind, dissipation by white-capping, resonant nonlinear interaction between the wave components, bottom friction and depth limited breaking. Wave diffraction is not included in the model, and at the scale of this study the translation of wave energy by this process is not relevant to the outcomes. A detailed description of the model equations, parameterizations, and numerical schemes can be found in Holthuijsen *et al*. (2004). All 3rd generation physics are included. The Collins friction scheme is used for wave dissipation by bottom friction, with a friction factor of 0.015.

The solution of the wavefield is found for the non-stationary (time-stepping) mode. Boundary conditions, wind forcing and resulting solutions are all time dependent, allowing the model to capture the growth, development and decay of the wavefield.

2.2 Bathymetry data

Bathymetry data was obtained from two sources. The NZ4631 chart was digitised and these data where incorporated with the nearshore profile data provided by Kapiti District Council.

2.3 Model domains

The hindcast utilised a two level nested domain. A coarse grid with resolution of 0.05° longitude by 0.05° latitude (~4km by 5km) covers the southern Taranaki and Cook Strait region and extends westwards into the Tasman Sea. The nested high resolution grid of 0.002° longitude by 0.002° latitude (~200m) was used for the Kapiti region. The two domains are shown in Figure 2.1.

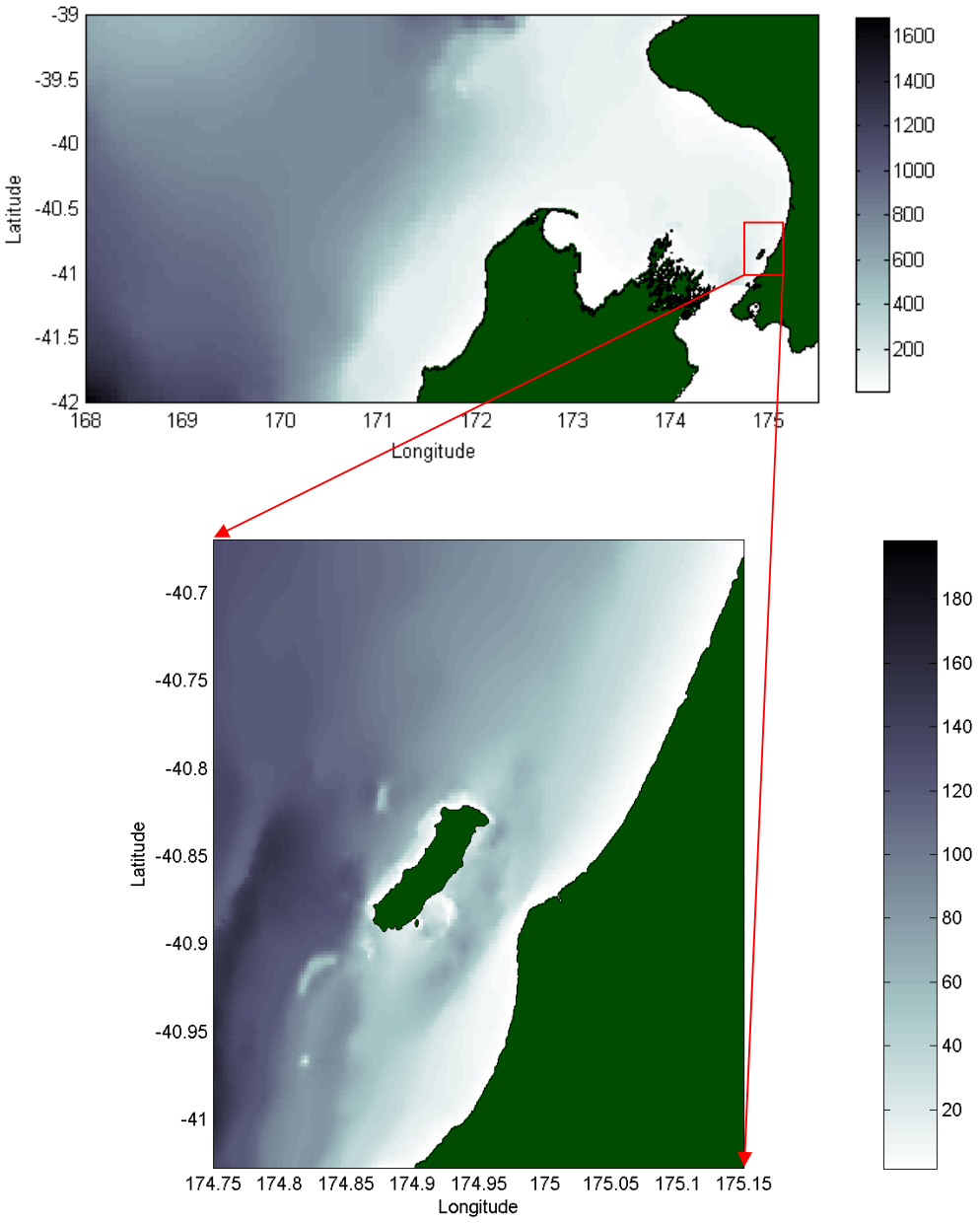

Figure 2.1 Wave model domains showing the coarse grid (top) and the high resolution Kapiti region grid (bottom).

2.4 Boundary conditions

The wave spectra on the open ocean boundaries of the coarse domain were obtained from archived nowcasts from NOAA WAVEWATCH III (NWW3). NWW3 is a state-of-the-art wave generation, propagation and transformation model for forecasting the evolution of directional wave energy spectra across the global oceans.

Along the open boundaries of the model domain, the primary statistical parameters of the incoming wavefield are interpolated from the NWW3 hindcast solution. Boundary spectra are then reconstructed by assuming a bi-modal Ochi-Hubble shape. Boundary conditions for the high resolution nested grid come directly from the coarse domain.

2.5 Winds

Generation of waves within the model domains occurs in response to wind forcing. A spatially varying wind field is specified from the blended NCEP re-analysis/QuikScat winds[1]. These data are 10 m wind velocity vectors in a 6-hourly gridded format at a resolution of 0.5° of longitude and latitude. The wind field is a combination of the ~12 hourly QuikScat satellite measurements and the NCEP global re-analysis (Milliff *et al*., 2004). The blended data product combines the benefits of measured satellite data with good spatial resolution and the continuous temporal coverage of the modelled re-analysis.

2.6 Model output

Waves were hindcast for the period from June 1997 to June 2006. An example of significant wave height across the high resolution grid is shown in Figure 2.2, which illustrates the significant variability in wave shoaling and refraction over

1 Data product from National Center for Atmospheric Research (NCAR)

the Kapiti area. A mean tide level (1 m above CD) was applied. Directional wave spectra were output at hourly intervals over the ten-year hindcast run for the range of locations as shown on Figure 2.3. Based on the model results, the most appropriate locations were selected to characterise the return period extrema (i.e. principally to avoid depth-limited wave breaking).

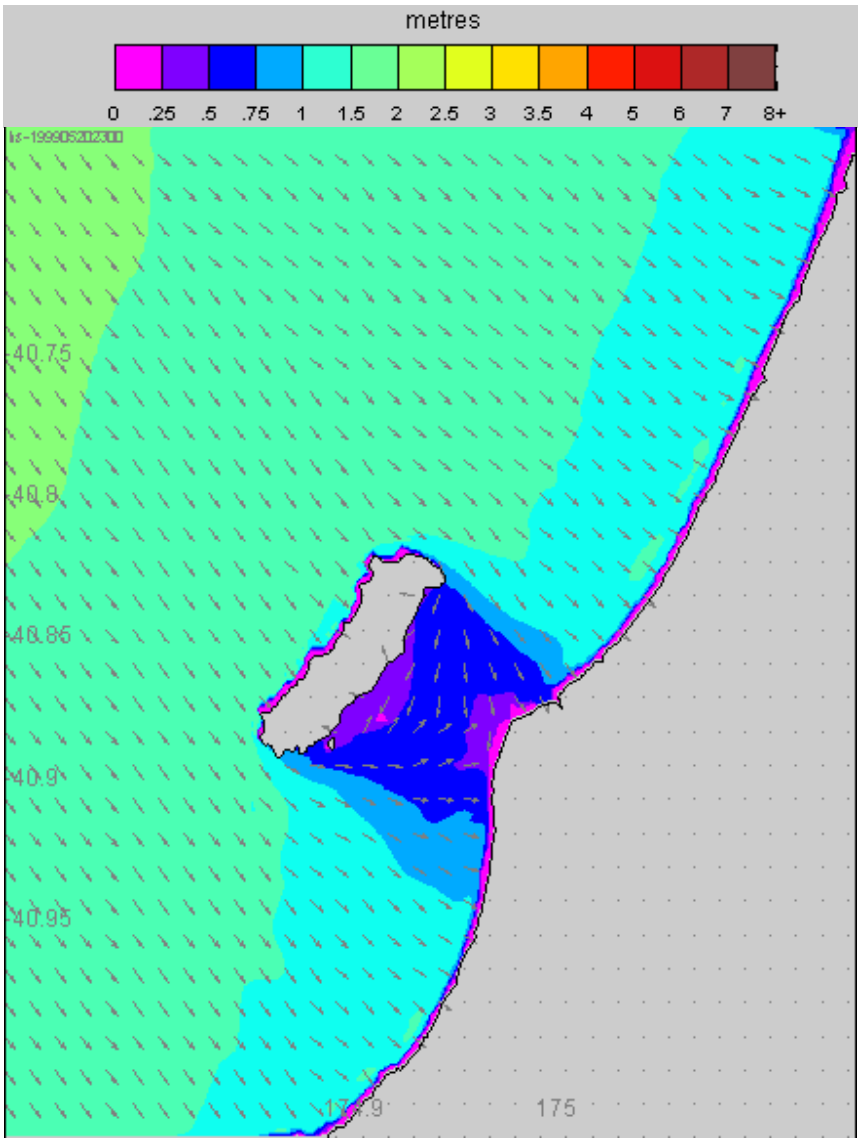

Figure 2.2 Example of hindcast significant wave height across the Kapiti Coast, in this case for a swell approaching from the northwest.

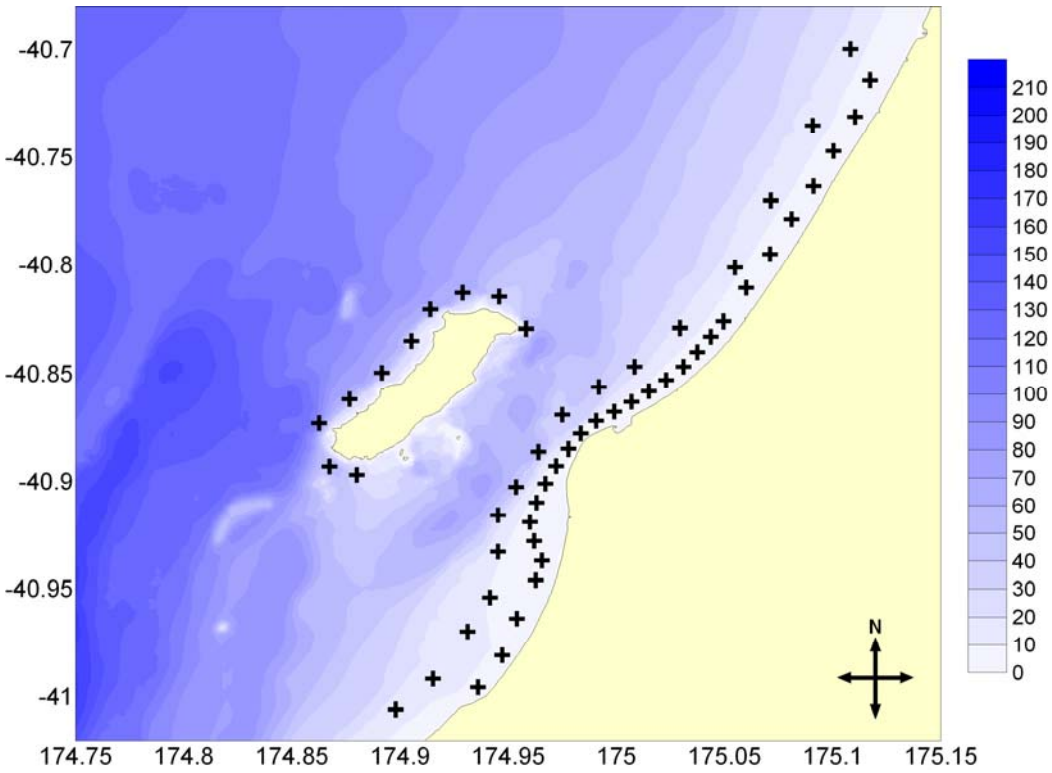

Figure 2.3 Wave hindcast locations, with depth contours in m relative to Chart Datum.

2.7 Model validation

Calibration and validation of the wave hindcast model physics have been undertaken at numerous locations around New Zealand. The closest validation locations are the Kupe Gas Field and the Maari Oil Field. A time-series validation plot, showing the measured and the modelled wave parameters from Kupe (~35 km south of Ohawe) is presented in Figure 2.4. A mean spectral wave period is shown in the validation plot, and it should be noted that the resolved wave period (either peak or mean) is very sensitive to the spectral shape. The hindcast model spectra is smooth continuum across the gravity wave frequency range, while the wave buoy response tends to attenuate the high frequency wave (i.e. <3 s). In the energetic conditions, the measured and modelled heights, periods and directions show very good correlation for this open water location. It is expected that an equivalent (or better) validation

would be attained for the Kapiti Coast, where the directional range is considerably narrower. However, onsite wave data would be needed for this validation.

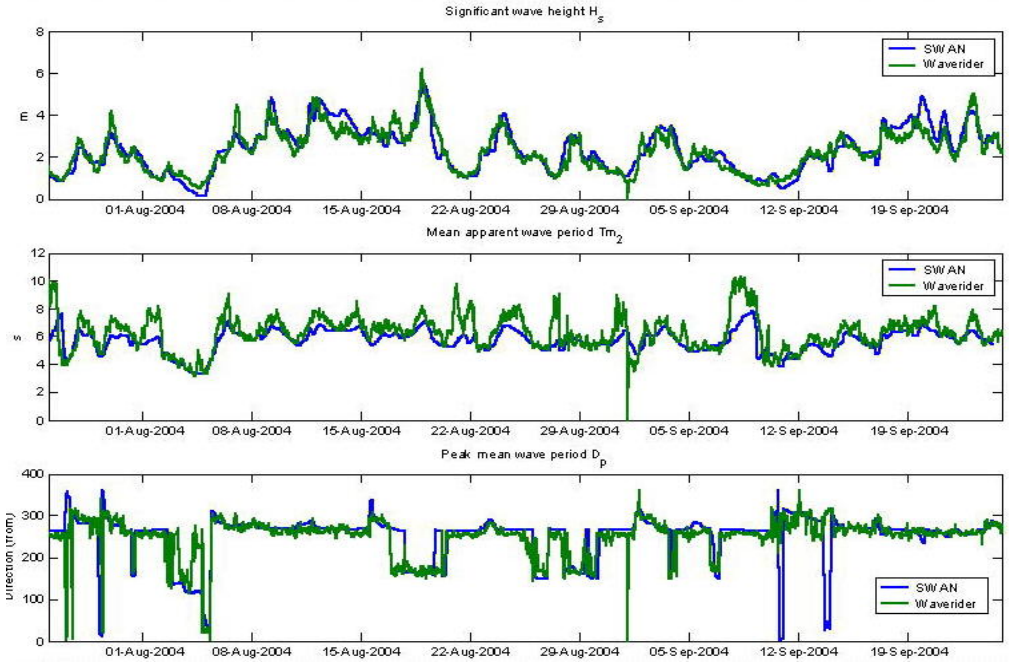

Figure 2.4 Hindcast time-series validation plot showing the measured and modelled wave data over a two-month period in 2004. Location is the Kupe Gas Field, South Taranaki.

3 DATA SOURCES - SEA LEVELS

Sea level, as measured by a sea-level recorder or tide gauge, has a number of components as follows:

- **Long Period Oscillations, MLOS.** Long-period (≥ 1 month) oscillations in sea-level arise from the effects of the annual cycle of temperature, large scale climate effects (like El Niño/Southern Oscillation and Interdecadal Pacific Oscillation), and rising sea level. We refer to this as the "mean level of the sea" (MLOS). It is different from mean sea level (MSL), which is a survey datum. MSL is often the MLOS for a particular year.
- **Storm Surge.** Storm surge has timescales between 36 and 360 hours. It is the response of the ocean to changing atmospheric pressure and wind.
- **Tides.** Tides have periods between 4 and 24 hours. They are the response of Earth's oceans to the gravitational attraction of the Moon and Sun.
- **Storm Tide.** Storm tide is the combined effect of storm surge and the tide. This is the water level that causes inundation. The tide is independent from storm surge (they are caused by completely different phenomena), though the highest water levels usually occur at high tide. This is because in New Zealand, high tide heights are generally much larger than storm surge heights, even in periods when the tidal range is low (e.g., neap tides).

3.1 Data

Three sets of data were used in the analysis of sea levels.

- **Sea Levels.** Sea levels were obtained from the NIWA sea-level recorder on the eastern side of Kapiti Island for the period from 23-Jul-1997 to 18-Dec-2006. The recorder is situated in the DOC boatshed. There is a gap of 25 days from 21-Jul-1999 to 15-Aug-1999 when the boatshed

was renovated and the recorder was moved. As a result of the move, the datum of the gauge shifted downwards by 0.198 m. To accommodate this, 0.198 m was subtracted from the early part of the record. The only other gap of more than 1 hour occurred between 27 and 31-Oct-2004.

- **Atmospheric Pressure** Atmospheric pressure was obtained from two sources: the barometer in NIWA's sea-level recorder station on Kapiti Island, and historical data from Paraparaumu Aerodrome. The Kapiti Island record is coincident with the sea-level data. The Paraparaumu Aerodrome dataset extends from 1-Dec-1961 to 31-Jul-1987 (when the Met Service was privatised). While this dataset is very old, it has been extensively used for numerous projects over the years, so its quality is guaranteed.
- **Weather** Weather, in the form of atmospheric pressure at mean sea level and 10 m winds at intervals of 1 degree in latitude and longitude, were obtained from the NOAA GFS model. The data are so-called "analyses", which are the initial conditions for the model at six-hourly intervals. Each analysis comprises data from previous forecasts, with data from instruments around the world assimilated into them. The record goes from March 2004 to January 2007. Notably, this is a lower resolution product than the blended NCEP re-analysis/QuikScat winds used in the wave modelling, however these data are used here for context rather than numerical simulation.

4 SPECIFIC ANALYTICAL METHODS

4.1 Spectral wave statistics

Given a directional wave spectrum $S(f,\theta)$, the 1-dimensional spectrum is obtained by integrating over directions:

$$S(f) = \int_0^{2\pi} S(f,\theta) d\theta \quad (1)$$

From the computed spectral energy density $S(f)$, the peak frequency f_p and peak energy $S_p = S(f_p)$ of the spectrum are located. Spectral moments

$$M_j = \int_0^{\infty} f^j S(f)\, df \quad (2)$$

are computed, allowing further statistics to be defined:

significant height $H_s = 4\sqrt{M_0}$ (3)

mean period $T_{m1} = M_0 / M_1$ (4)

mean apparent period $T_{m2} = \sqrt{M_0 / M_2}$ (5)

mean frequency $f_{mean} = M_1 / M_0$ (6)

mean crest period $T_{cr} = \sqrt{M_2 / M_4}$ (7)

spectral width $SW = 1 - \frac{{M_2}^2}{M_0 M_4}$ (8)

T_{m2} is often used as a spectral approximation of the zero-down-crossing period statistics Tz. Directional moments are:

$$M_c = \int_0^{\infty}\int_0^{2\pi} S(f,\theta)\cos\theta \; d\theta \, df \quad (9)$$

$$M_s = \int_0^{\infty}\int_0^{2\pi} S(f,\theta)\sin\theta \; d\theta \, df \quad (10)$$

The mean direction is $\theta_0 = \arctan\left(\frac{M_s}{M_c}\right)$ (11)

The wave periodicity associated with the energetic wave events was estimated from the mean of the peak spectral wave periods from the upper 1% of the significant wave events.

4.2 Evaluation of extrema

There are a number of different probability distribution functions that can be used to find a best fit to available data in the estimation of the extrema. The Fisher-Tippett Type I distributions were derived from statistical theory of extremes, and hence are true extremal distributions. The Weibull distribution with k = 2 is equivalent to the Rayleigh distribution. The parameters A, B, and k (Table 4.1) are known as the scale, location, and shape parameters, respectively. Of the distributions shown in Table 4.1, choosing the Weibull distribution with k = 0.75 clearly leads to the highest extremal estimates. Choosing the Weibull distribution with k=2.0 leads to the lowest estimates. The FT-I distribution gives estimates intermediate to the Weibull with k values of 1.0 and 1.4 (Leenknecht *et al*. 1991).

The key skill in defining the extrema comes from selecting data for analysis, estimating parameters in the distribution function, and choosing an appropriate extremal distribution function. Each of these choices can significantly influence the estimated extreme values, especially those for very rare events (Leenknecht *et al.* 1991). There is no strong theoretical reason for preferring one distribution function over another. The single sample cannot be expected to fit the true distribution function exactly, especially for the few largest events. For processes such as significant wave heights and current velocities, a best-fitting distribution function is often chosen from among several candidates. Three alternatives for determining the fit of a distribution function are, the least squares method, the maximum likelihood method, and the method of moments. The least squares method is simplest and, with two-parameter distribution functions, it is often used. Regardless of the method used, it is prudent to plot

the computed distribution function and data together and ensure that the fit is consistent.

Table 4.1 Equations commonly used to describe the distribution of storm event wave heights for extrapolation to determine wave extrema (Leenknecht *et al.* 1991).

Distribution Function	Mathematical Expression	Mean & Standard Deviation	Parameters
Fisher-Tippett I (FT-I) or Gumbel	$F(x) = e^{-e^{-\left(\frac{x-B}{A}\right)}}$	$\bar{x} = B + 0.5772A$ $\sigma = 1.283A$	$A = 0.779\sigma_x$ $B = \bar{x} - 0.4500\ \sigma_x$
Weibull	$F(x) = 1 - e^{-\left(\frac{x-B}{A}\right)^k}$ *general*	$\bar{x} = B + A\,\Gamma\left(1 + \frac{1}{k}\right)$ $\sigma_x = A\sqrt{\Gamma\left(1 + \frac{2}{k}\right) - \Gamma^2\left(1 + \frac{1}{k}\right)}$	
	$k = 0.75$	$\bar{x} = B + 1.191A$ $\sigma_x = 1.611A$	$A = 0.621\sigma_x$ $B = \bar{x} - 0.740\sigma_x$
	$k = 1.0$	$\bar{x} = B + A$ $\sigma_x = A$	$A = \sigma_x$ $B = \bar{x} - \sigma_x$
	$k = 1.4$	$\bar{x} = B + 0.911A$ $\sigma_x = 0.660A$	$A = 1.515\sigma_x$ $B = \bar{x} - 1.380\sigma_x$
	$k = 2.0$	$\bar{x} = B + 0.886A$ $\sigma_x = 0.463A$	$A = 2.160\sigma_x$ $B = \bar{x} - 1.914\sigma_x$

4.2.1 Return period wave heights

For the estimation of the return period significant wave heights, the Peaks over Threshold (POT) data selection method was used, and applying a 75th percentile exceedence level as the threshold. Two types of model distributions were used; the 3-parameter Weibull distribution (shape parameters of $0.5 < k < 3.0$) and the Fisher-Tippet Type 1 distribution. The least-squares method was been used to determine the most suitable distribution function that describes the hindcast wave data distribution. Where the fit to the Weibull and Fisher-Tippet distributions were close, the more conservative Fisher-Tippet distribution was selected.

4.3 Water level analysis methods

4.3.1 Tidal Analysis

Tidal analysis involves fitting constituents to the sea-level signal. Each constituent is associated with an astronomical phenomenon that has a particular period which can be identified very precisely. For example, the semidiurnal solar constituent, S_2, arises from the direct gravitational attraction of the Sun on Earth's water. It has a period of exactly 12 hours. The symbol, S_2, is called a Darwin symbol, devised by Sir George Darwin (a son of Charles Darwin) in the 1890s. The symbols contain a letter and a number. The letter denotes the phenomenon (S for Sun, M for Moon, etc), and the number denotes the number of tides per day (2 for semidiurnal, 1 for diurnal, etc). Tidal analysis calculates the amplitude and phase of each of these constituents. In this project, the t_tide package of Pawlowicz et al (2002) was used. Statistical significance was determined by means of a constituent's signal-to-noise ratio (SNR), which was defined as the square of the amplitude divided by its 95% confidence interval. Only constituents with SNR greater than 10 were considered significant.

4.3.2 Storm Surge

Storm surge was calculated from the sea-level record in the following steps:

- Calculate the tide from its constituents and subtract from the record, producing the "residual".
- Removes spikes from the residual and replace them with gaps.
- Interpolate across the gaps.
- Band-pass filter the de-spiked, de-gapped residual.
- Reintroduce the gaps.

The de-spiking routine was based on the method of Goring & Nikora (2001). The band-pass filter was based on orthogonal wavelet decomposition (see, e.g., Misiti *et a*l 2000) in which the signal is decomposed using a basis function called the "mother wavelet". There are many mother wavelets available. The

one used here is shown in Figure 4.1. It is one of the Daubechies family, after Daubechies(1988). A relatively non-mathematical explanation of wavelets and the history of their development is available in Hubbarb (1996).

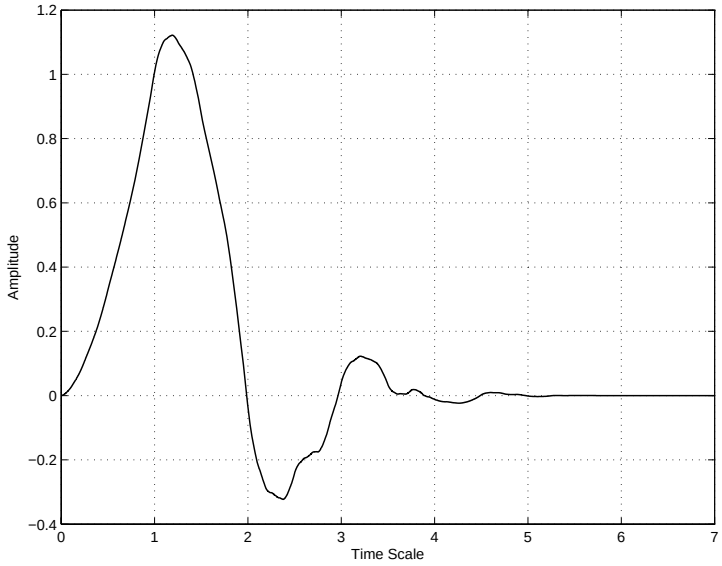

Figure 4.1 Daubechies No 4 (db4) mother wavelet.

The way the orthogonal wavelet decomposition works is that the mother wavelet is fitted to the signal, generating a detail and an approximation. The mother wavelet is then dilated (its timescale is doubled) and fitted to the approximation, producing another detail and approximation. And this process is repeated until the mother wavelet extends to the length of the record. The resulting wavelet details are orthogonal which means they can be combined with each other in any manner, and each has a timescale that is double the previous one. For band-pass filtering, we simply combine the details with the timescales of interest. In the case of hourly data, the wavelet details have the following periods (in hours): 3, 6, 12, 24, 48, 96, 192, 384, 768,…. For storm surge, we combine wavelet details 5 to 8 representing timescales from 48 to 384 hours.

The advantage of this method of low-pass filtering over traditional methods such as the tapered boxcar method of Goring & Bell (1996) is that it is applicable to signals that are non-stationary. Stationarity is the property that the

variance (2^{nd} statistical moment) is constant, no matter what window is used. Residual sea-level is not stationary, as will be shown. The main difference from traditional methods, is that they are global (the same transformation is applied to the entire record, no matter what its contents), whereas orthogonal wavelet decomposition is localised. For storm surge, this means that local features such as a steepening in the vicinity of the crest of an event is allowed through, whereas with traditional methods it would be smoothed off.

4.3.3 Inverted Barometer

Inverted barometer (IB) is a theoretical concept, being the direct response of the static ocean to changing atmospheric pressure. In an ideal ocean, far from land:

- For every hPa rise in atmospheric pressure, sea level falls by 1 cm; and
- For every hPa fall in atmospheric pressure, sea level rises by 1 cm.

In practice, near the coast, this relationship is far from exact because of the influence of wind and coastal trapped waves. The latter are waves between the shoreline and the continental shelf that in the Southern Hemisphere propagate around landmasses with the land on their left. Inverted barometer is calculated from the atmospheric pressure record by subtracting pressure from its mean and multiplying by 10 to give mm of sea level. The signal is then processed in the same manner as storm surge (omitting subtraction of the tide).

4.3.4 Mean Level of the Sea (MLOS)

MLOS is calculated by low-pass filtering the de-spiked, de-gapped residual described above. In practice this amounts to using the wavelet approximation at level 8, meaning that MLOS contains timescales of 768 hours and longer.

An important use of MLOS is in relating levels between sites. Usually, MLOS is constant over a wide range of the ocean, so by assuming it is constant between two sites, we can transfer the survey datum from one place to another. KDC uses Wellington Chart Datum (WCD) as its survey datum. Kapiti island sea-level recorder has its own datum, KICD. The 2003/04 Nautical Almanac

indicates that the MLOS for 2000 at Wellington was 1.11 m above WCD. Therefore, we can relate the sea levels at Kapiti Island sea-level recorder to WCD as follows:

Kapiti Sea Levels (WCD) = Kapiti Sea Levels (KICD) – MLOS for 2000 + 1.11

Alternatively, to obtain Kapiti coast sea levels to MSL datum, omit the 1.11 addition and use:

Kapiti Sea Levels (MSL) = Kapiti Island Sea Levels (KICD) – MLOS for 2000.

4.3.5 Joint Probability: tide and storm surge or storm tide

Inundation from the ocean usually occurs when high sea levels combine with large waves. High sea levels occur when a large tide coincides with moderate or large storm surge. However, if a large storm surge occurs at a time of apogean neap tides, when the tidal range is very small, flooding is unlikely to occur. On the other hand, if even a small storm surge occurs at a time of perigean spring tides when the tidal range is very large, there may be flooding. To unravel this complexity, Tawn & Vassie (1991) developed the joint probability method (JPM) in which the annual exceedence probability of combined tide and storm surge is calculated by integrating the probability density functions of both phenomena. Later, they modified the method to better account for the statistics at the tails of the distributions and called it the revised joint probability method (RJPM). This is the method that has been used in this study.

The package for the JPM and RJPM is called ExtLev and is available from the NIWA website (www.niwa.co.nz). The algorithms in ExtLev for separating tide and storm surge are inferior to those used in this study, so a special signal was prepared for ExtLev by combining forecast tide and calculated storm surge. This ensured that the storm surge used in ExtLev was the same storm surge as used in this study.

An alternative to the JPM and RJPM which were developed for UK conditions is the"empirical simulation technique" (EST) developed by Scheffner et al (1996) for the Gulf of Mexico. In this method, empirical cumulative distribution functions (CDFs) are calculated for high tide and storm surge events above a threshold, then the average number of storm surge events per year, λ, is used to calibrate the Poisson distribution:

$$p(s;\lambda) = \frac{\lambda^s e^{-\lambda}}{s!} \qquad (12)$$

where *s* is the number of events for a given year, and *p* is the probability of that occurring. Equation 12 is used to obtain the probability distribution function which is then integrated numerically to produce the CDF. The joint probability of storm tide is then calculated for various return periods using a Monte Carlo procedure with the following steps for each year of simulation:

- Draw a random number of events per year, *n*, from the Poisson CDF;
- Draw *n* storm surge heights from the storm surge events CDF;
- Draw *n* high tide heights from the high tide CDF;
- Add the storm surge and high tide heights to produce *n* storm tides for the year;
- Find the maximum storm tide for the year.

The process is repeated for the number of years return period (RP) under consideration and the maximum over all the years is determined. For example, for the 10-year RP, the above steps are repeated 10 times and the maximum of the 10 annual maxima is found. The whole procedure is repeated enough times for the standard error of the estimated RP to lie below the precision of the result. In other words, if the precision of the result is 1 cm, then the procedure is repeated enough times for the standard error to fall to 1 mm. Typically, for 1-year RP, the number of simulation runs is 10,000 representing the mean annual RP over 10,000 years, but for 100-year RP, it is usually only 100.

Drawing a random number from a CDF is done using a method called "nonparametric bootstrapping". This simply involves obtaining a uniformly

distributed number between 0 and 1 and finding the corresponding variable from the CDF using interpolation.

4.3.6 Joint Probability of Waves and Storm Tide

The EST procedure outlined in Section 4.3.5 is used for calculating the joint probability of waves and storm tide, with wave events replacing storm surge events as the driver for the number of events per year.

5 WAVE RESULTS

The hindcast time-series data were analysed to select the most appropriate sites to characterise the extreme wave conditions. The main criterion in this process is to ensure that under storm conditions, the modelled wave heights are not depth-limited due to breaking. The higher-order significant wave height statistics (i.e. maximum, 99th and 95th percentiles) were compared for all the output locations (see Fig. 2.3), and these data were used to select the best sites. The maximum significant wave heights are plotted on Figure 5.1, showing the wave height attenuation in the nearshore locations.

The selected sites are shown on Figure 5.2, and the details are given in Table 5.1. Notably, a near-constant distance offshore was selected as the best series of locations for the study, rather than along a given contour. Howver, the steep seabed gradients along the shore in the lee of Kapiti Island mean that the water depths at these locations are greater than on the low gradient nearshore regions to the north and south. This does not significantly influence the wave results in terms of the storm wave height extrema for design.

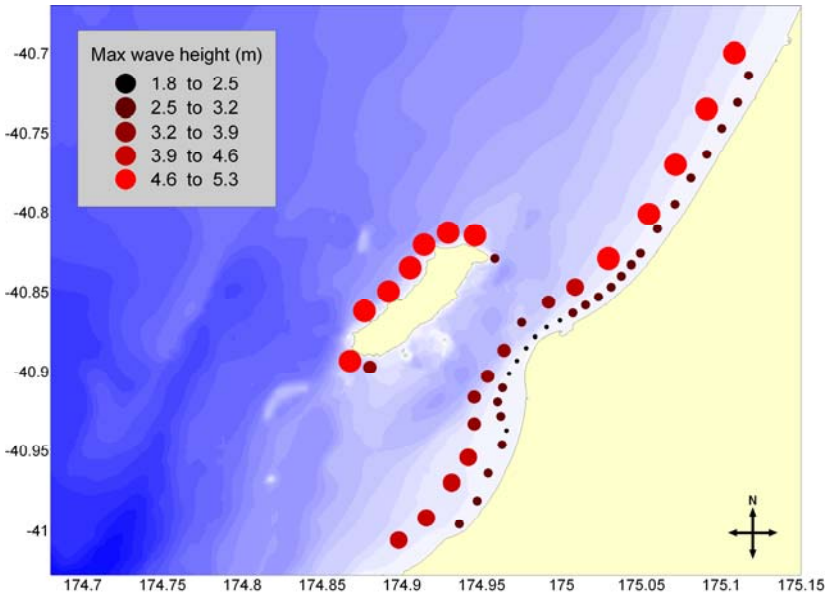

Figure 5.1 The maximum modelled significant wave height.

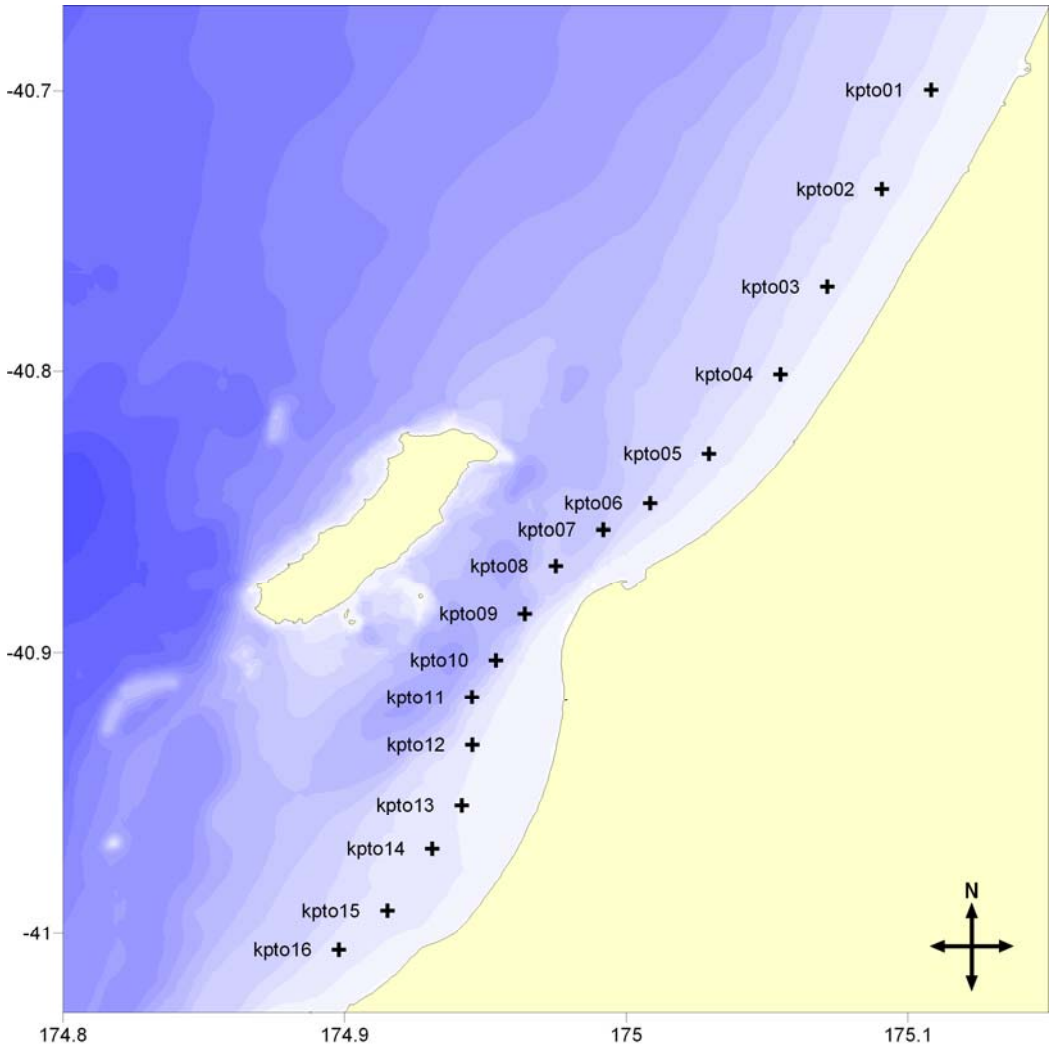

Figure 5.2 Wave hindcast output locations

Table 5.1 Wave hindcast locations for the design statistics

Name	Lat	Long	Depth (CD,m)
kpto01	175.1082	-40.699675	14.99
kpto02	175.09072	-40.735072	15.1
kpto03	175.07133	-40.770079	14.73
kpto04	175.05474	-40.801123	12.82
kpto05	175.02939	-40.829031	18.36
kpto06	175.00843	-40.846905	24.93
kpto07	174.99185	-40.856312	38.94
kpto08	174.97495	-40.869168	35.29
kpto09	174.96399	-40.886414	48.16
kpto10	174.95367	-40.90272	41.35
kpto11	174.94522	-40.91589	33.81
kpto12	174.94532	-40.932825	12.17
kpto13	174.94157	-40.954063	9.37
kpto14	174.93114	-40.969825	12.87
kpto15	174.91518	-40.991775	16.11
kpto16	174.89797	-41.005886	15.38

5.1 Design significant wave height statistics

The design wave height statistics are provided in Table 5.2. Max Hs is the largest significant wave height modelled in the 10-year hindcast, and P99 and P95 relate to the 99th and 95th percentile level for the significant wave heights in the time-series. The P99 wave direction is the mean direction (coming from, DegT) for the upper 1% of the wave heights, and can be used to characterise the typical wave direction associated with storm events (also shown on Fig. 5.3). The peak spectral wave period associated with the storm events (P99 Tp) is the mean Tp from the upper 1% of the wave height events. Notably, the P99 Tp is a mean value and the actual range of Tp values for the energetic wave events should be applied for design. The joint probability tables in the appendix to this report should be used for this purpose.

The significant wave height extrema at 1-month to 100-year return periods are provided in Table 5.2, and the 1-100 year values are also plotted on the regional map in Figures 5.4 – 5.7.

The reliability of the predicted return period values is directly related to the accuracy of the source data and the duration of the time-series. Also, it is implicit that the environmental conditions over the data period will be

representative of the project lifetime, which is a reasonable assumption in this application. As a rule-of-thumb, three times the data duration is considered to provide an acceptable extrapolation period for defining the extrema (Leenknecht *et al*, 1991). On this basis, the 30-year return period value can reliably be defined from extrapolation of the hindcast data available.

Table 5.2 Summary design significant wave heights for the Kapiti Coast

Name	Max Hs (m)	P95 Hs (m)	P99 Hs (m)	P99 Direction	P99 Tp (s)	1-mth RPV (m)	3-mth RPV (m)	6-mth RPV (m)	1-yr RPV (m)	2-yr RPV (m)	10-yr RPV (m)	50-yr RPV (m)	100-yr RPV (m)
kpto01	4.75	2.60	3.33	291	9.11	2.83	3.44	3.79	4.11	4.42	5.09	5.70	5.95
kpto02	4.83	2.63	3.36	293	9.14	2.86	3.48	3.82	4.15	4.46	5.14	5.75	5.99
kpto03	4.74	2.57	3.27	297	9.05	2.80	3.4	3.74	4.05	4.36	5.01	5.60	5.84
kpto04	4.7	2.52	3.2	299	9.07	2.74	3.32	3.64	3.95	4.24	4.87	5.45	5.68
kpto05	4.63	2.42	3.06	307	8.93	2.65	3.22	3.54	3.84	4.12	4.74	5.30	5.52
kpto06	3.92	2.07	2.57	319	8.37	2.28	2.76	3.03	3.28	3.52	4.03	4.50	4.69
kpto07	3.31	1.74	2.15	330	7.57	1.93	2.33	2.56	2.77	2.98	3.41	3.81	3.97
kpto08	3.13	1.43	1.75	324	5.88	1.6	1.90	2.08	2.24	2.40	2.73	3.04	3.16
kpto09	3.29	1.41	1.76	267	5.61	1.58	1.89	2.07	2.25	2.42	2.79	3.14	3.28
kpto10	3.27	1.61	2.05	267	6.99	1.78	2.17	2.38	2.59	2.79	3.22	3.62	3.79
kpto11	3.42	1.86	2.4	278	7.91	2.06	2.51	2.76	3.00	3.23	3.71	4.16	4.34
kpto12	3.62	2	2.54	288	8.32	2.19	2.65	2.90	3.15	3.38	3.87	4.33	4.51
kpto13	3.92	2.17	2.77	293	8.71	2.36	2.85	3.12	3.38	3.62	4.15	4.63	4.83
kpto14	4.38	2.3	2.95	297	8.69	2.54	3.08	3.38	3.67	3.94	4.53	5.07	5.29
kpto15	4.53	2.36	3.01	303	8.57	2.63	3.19	3.50	3.80	4.08	4.69	5.24	5.46
kpto16	4.59	2.38	3.04	308	8.54	2.66	3.22	3.53	3.83	4.11	4.72	5.28	5.50

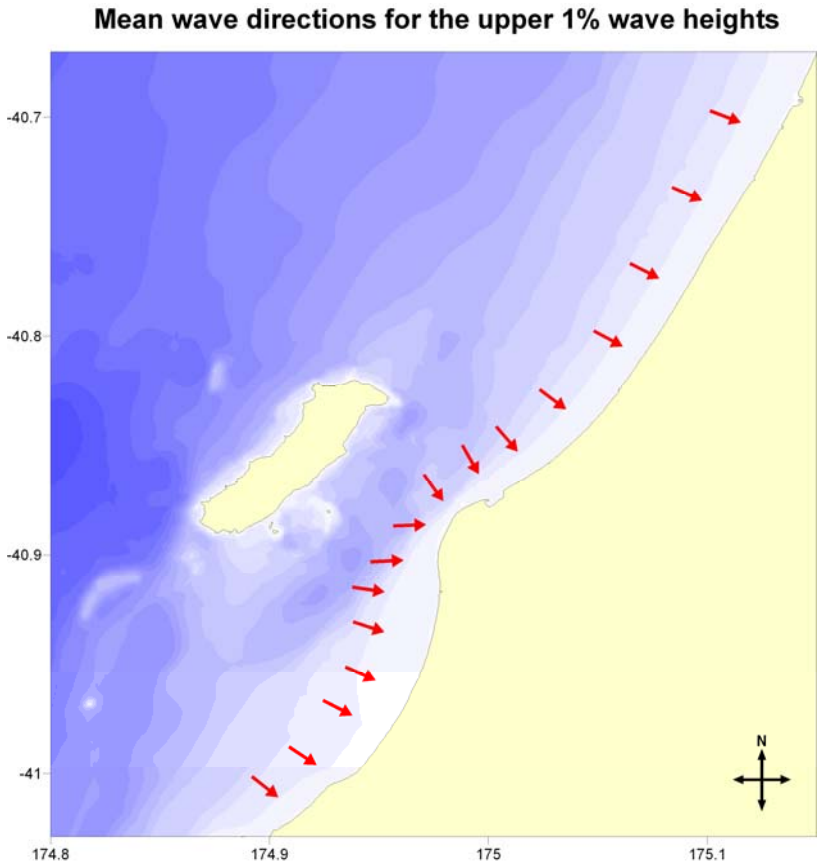

Figure 5.3 The wave directions associated with the storm events.

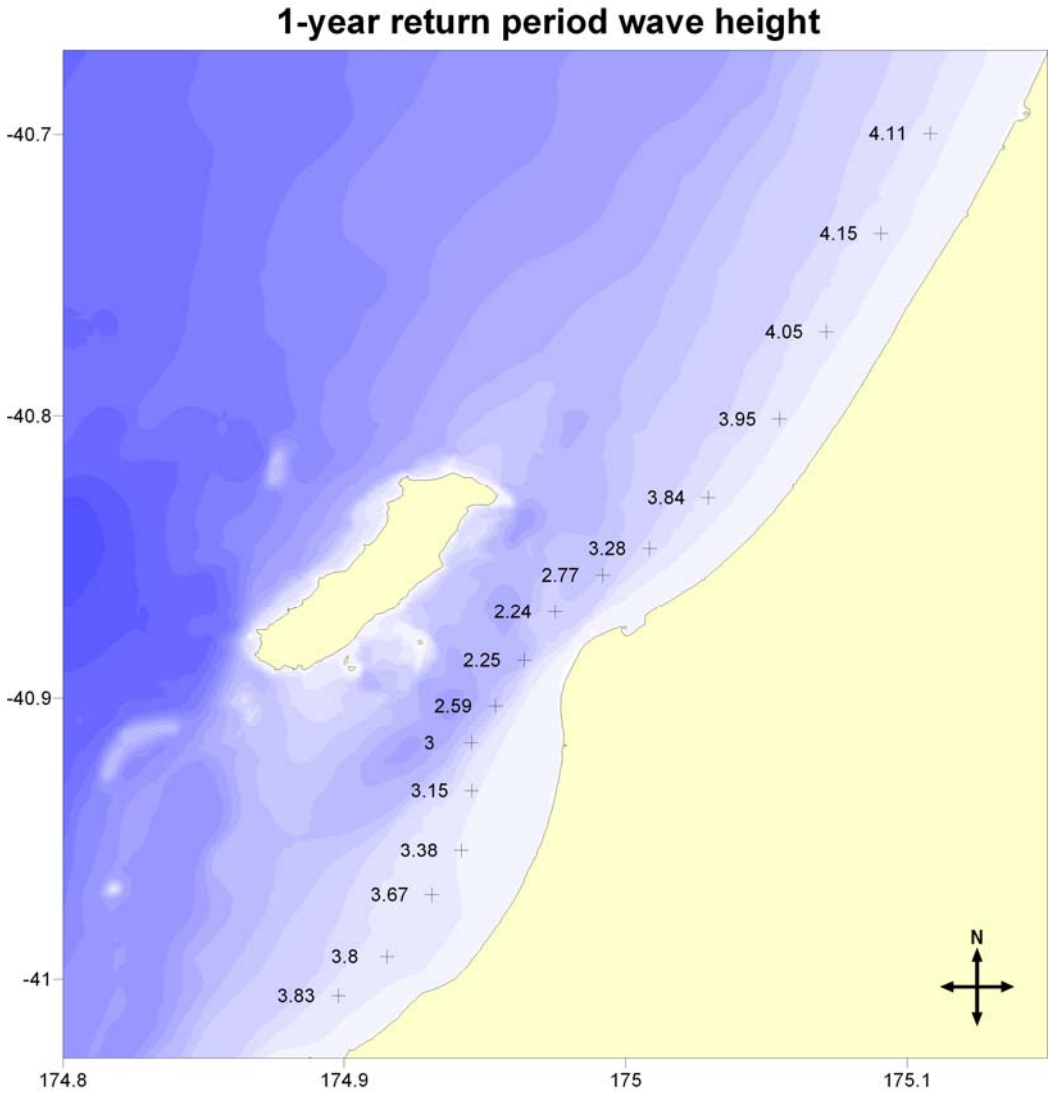

Figure 5.4 The design 1-year return period significant wave height for the Kapiti Coast

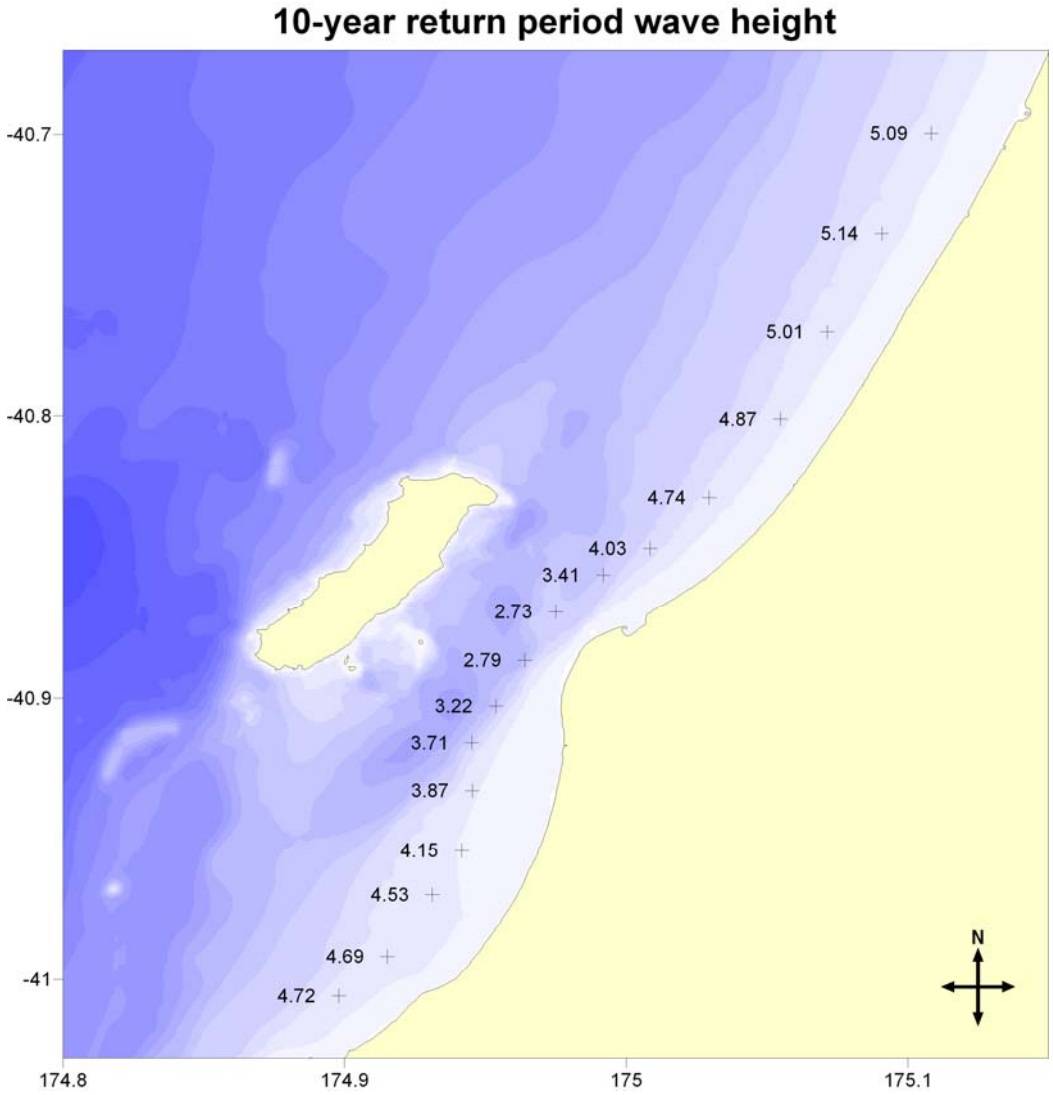

Figure 5.5 The design 10-year return period significant wave height for the Kapiti Coast

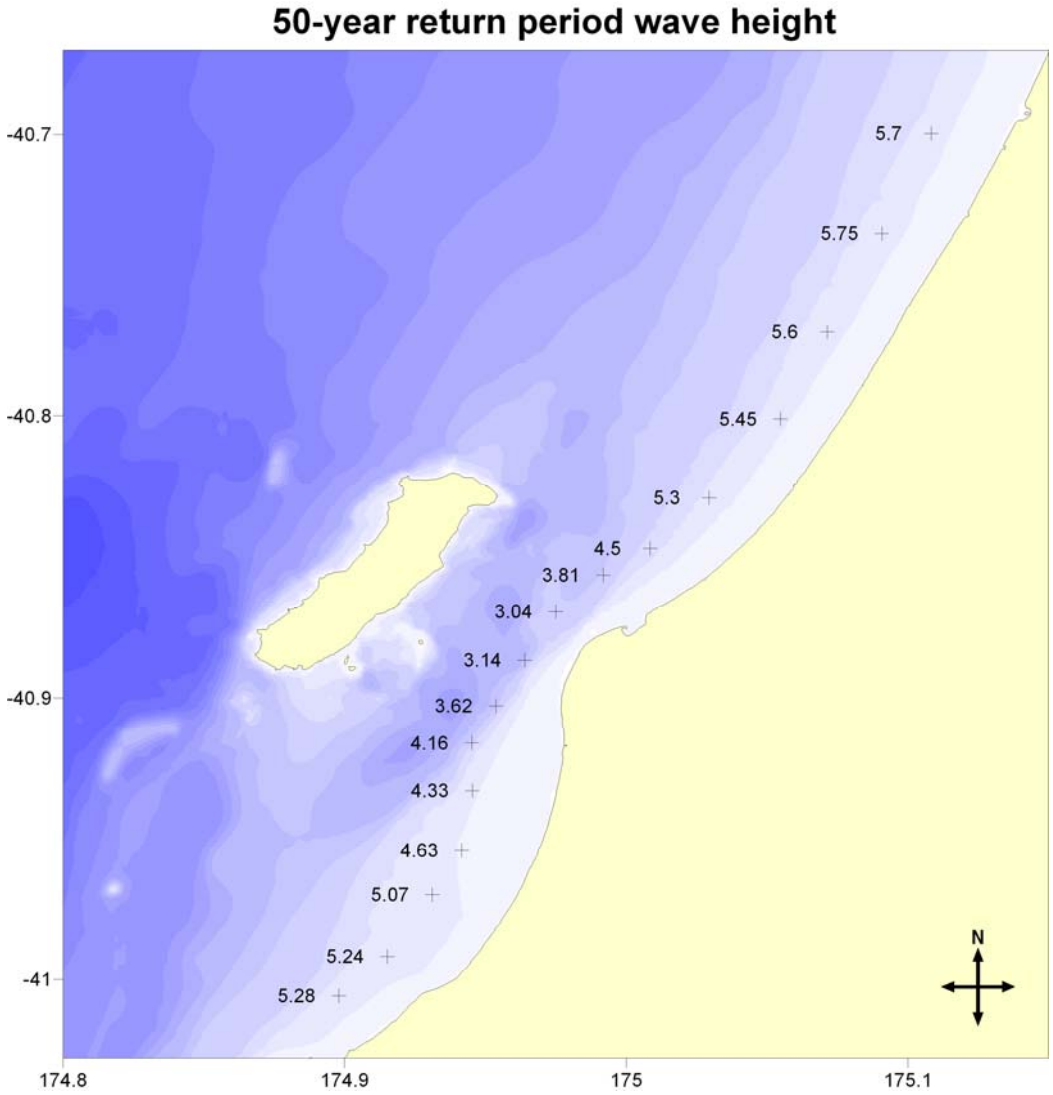

Figure 5.6 The design 50-year return period significant wave height for the Kapiti Coast

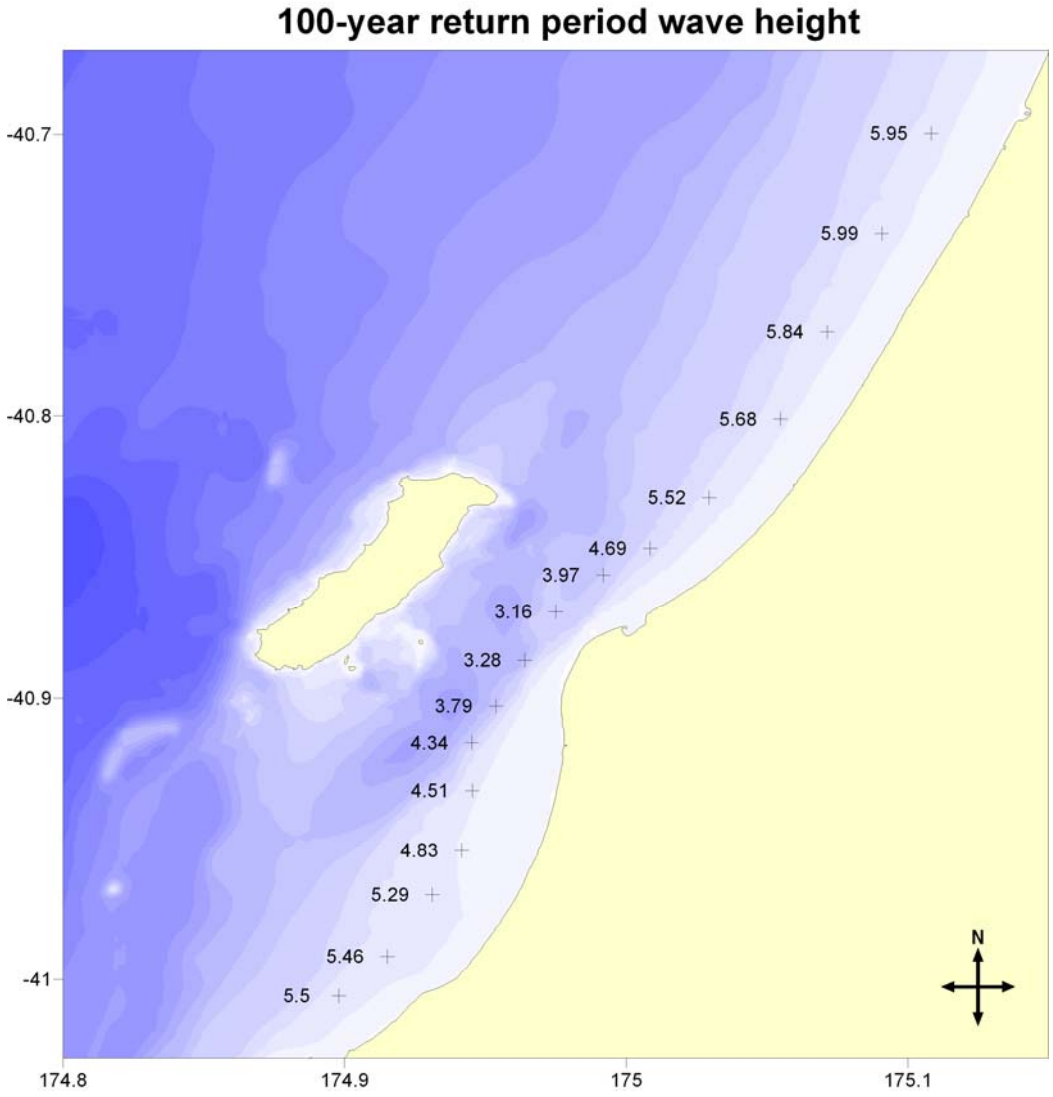

Figure 5.7 The design 100-year return period significant wave height for the Kapiti Coast

The joint probability distribution of the significant wave height, mean wave direction and the peak spectral wave period for each location are appended to this report in an electronic form:

[KDC wave joint probability data MSL_March_2007.xls].

Table 5.3 Monthly and annual significant wave height (m) statistics for the hindcast locations

	Kpto16	Kpto15	Kpto14	Kpto13	Kpto12	Kpto11	Kpto10	Kpto9	Kpto8	Kpto7	Kpto6	Kpto5	Kpto4	Kpto3	Kpto2	Kpto1
Mean	1.04	1.04	1.03	0.99	0.92	0.86	0.75	0.67	0.68	0.81	0.94	1.11	1.16	1.20	1.23	1.23
Median	0.87	0.87	0.88	0.85	0.80	0.74	0.65	0.59	0.60	0.70	0.81	0.96	1.01	1.05	1.08	1.08
Max	4.59	4.53	4.38	3.92	3.62	3.42	3.27	3.29	3.13	3.31	3.92	4.63	4.70	4.74	4.83	4.75
95%	2.38	2.36	2.30	2.17	2.00	1.86	1.61	1.41	1.43	1.74	2.07	2.42	2.52	2.57	2.63	2.60
99%	3.04	3.01	2.95	2.77	2.54	2.40	2.05	1.76	1.75	2.15	2.57	3.06	3.20	3.27	3.36	3.33
January mean	0.89	0.89	0.88	0.84	0.78	0.72	0.62	0.56	0.59	0.70	0.81	0.95	1.00	1.03	1.05	1.05
February mean	0.89	0.89	0.88	0.84	0.79	0.74	0.65	0.59	0.61	0.72	0.83	0.96	1.00	1.04	1.06	1.06
March mean	0.84	0.84	0.83	0.80	0.75	0.70	0.60	0.53	0.55	0.65	0.76	0.90	0.94	0.97	1.00	1.00
April mean	0.80	0.81	0.81	0.78	0.74	0.69	0.61	0.55	0.56	0.65	0.75	0.88	0.93	0.96	0.99	1.00
May mean	1.08	1.08	1.08	1.03	0.96	0.90	0.79	0.70	0.70	0.83	0.98	1.16	1.21	1.25	1.29	1.29
June mean	1.26	1.26	1.25	1.19	1.11	1.04	0.90	0.80	0.82	0.97	1.13	1.34	1.40	1.45	1.48	1.47
July mean	0.96	0.96	0.96	0.93	0.87	0.82	0.73	0.66	0.67	0.78	0.89	1.05	1.10	1.14	1.17	1.17
August mean	1.07	1.08	1.08	1.04	0.97	0.91	0.80	0.72	0.74	0.85	0.99	1.17	1.23	1.27	1.31	1.31
September mean	1.30	1.29	1.27	1.21	1.12	1.03	0.88	0.78	0.81	0.98	1.15	1.36	1.43	1.47	1.50	1.49
October mean	1.24	1.23	1.22	1.16	1.07	0.99	0.86	0.76	0.79	0.95	1.12	1.32	1.38	1.41	1.45	1.44
November mean	1.02	1.02	1.02	0.98	0.93	0.88	0.76	0.67	0.68	0.81	0.93	1.09	1.14	1.18	1.22	1.22
December mean	1.11	1.10	1.08	1.03	0.95	0.88	0.76	0.67	0.70	0.85	0.99	1.16	1.20	1.23	1.26	1.25

6 WATER LEVEL RESULTS

In this section, the overall characteristics of the sea-level and pressure records are considered using Fourier spectra, followed by an examination of the individual components of tide, storm surge, and mean level of the sea (MLOS). Within those components, we also consider their interaction.

6.1 Fourier Spectra

The Fourier spectra for sea level, residual (sea level less tides), and atmospheric pressure are presented in Figure 6.1. The spectra reveal a great deal of information about the signals that are being analysed, as follows:

The spikes in sea level are the tide. The spikes in the residual are the part of the tide signal that cannot be identified as tide. Some of these occur because the signal varies with time, whereas tides are constant with time. Others, especially those at frequencies larger than 40 °/h occur because of nonlinear interaction between the main tidal constituents.

The spikes in the pressure spectrum are atmospheric tides. They have periods that are multiples of 24 hours. There is also a tiny spike just to the left of the main component at 30 °/h (12-hour period) which is the effect of the Moon. Atmospheric tides are caused by absorption of water vapour in the stratosphere.

The region of the spectrum between 1 and 10 °/h is the storm surge region. The slopes of the curves of sea level and pressure in this region are quite important in characterising the fractal nature of the two signals because they define the Hurst parameter, H, which determines the persistence of the signal, and whether or not the past can be used to forecast the future. The Hurst parameter takes values between 0 and 1. If $H > 0.5$, the signal is persistent and past values can be used to forecast the future, but if $H < 0.5$, past values cannot be used to forecast the future. The pressure signal has $H = 0.50$ and the sea-level signal has $H = 0.23$, so neither can be used for forecasting.

The flattish portion of the spectrum from the y-axis to 1 °/h defines the mean level of the sea (MLOS). Because it is flat, it appears to be random fluctuations

(white noise). This is the result of many different processes with different periods and strengths interacting in different ways.

Fourier spectra are plotted on log-log axes by convention, but this masks the huge effect of the semidiurnal tides on the signal, while exaggerating the importance of the residual. Table 6.1, showing the energy in the various bands of the spectrum for the raw signal and the residual, puts it in perspective. However, while the energy for storm surge is small (2.5% of the total), it is episodic, whereas the other phenomena are ubiquitous. Thus, storm surge events can have a major influence on sea level.

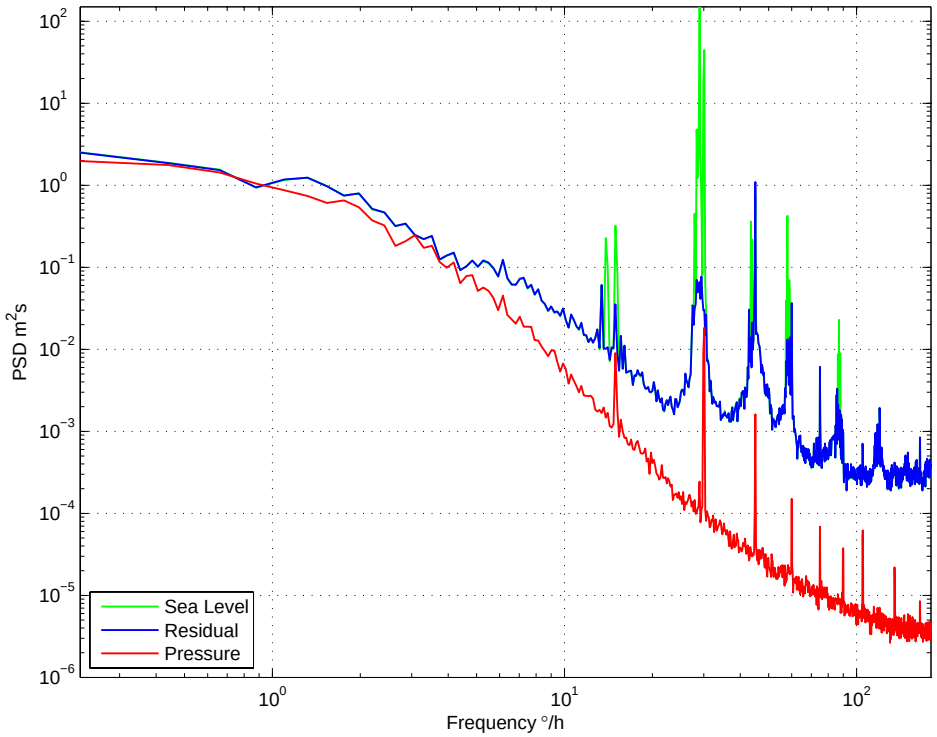

Figure 6.1 Fourier spectra for sea level, residual (sea level less tides), and atmospheric pressure.

Table 6.1 Energy (dm^2) in the various bands in the spectrum

Phenomenon	Raw	Residual
MLOS	49	49
Storm Surge	51	51
Diurnal Tides	7	3
Semidiurnal Tides	1939	5
Shallow Water Tides	17	12
Total	2063	120

6.2 Tide

The results of annual analyses of the 9 years of record are presented in Table 6.2, in which the constituents for the measured duration have been converted from amplitude and phase to complex numbers, averaged, then converted back to amplitude and phase. Points arising from this table are:

- The most important constituent is the semidiurnal lunar tide, M_2, having an amplitude that is twice the size of the next largest, the solar semidiurnal tide, S_2. The combinations of these leads to a strong fortnightly spring/neap effect.
- There are only two diurnal tides and they are weak, leading to little variation in amplitude between morning and afternoon tides.
- The relatively small semidiurnal elliptic tide, N_2, means there is only a weak monthly perigean/apogean effect.
- The large number of shallow water tides indicates there is considerable interaction between the major tides as they propagate to this location.

The tidal parameters calculated by synthesizing the constituents in Table 6.2 for a tidal epoch (18.6 years) are listed in Tables 6.3 and 6.4. The first two columns define the parameter. The third column has the level of the parameter in m above WCD and the fourth column has the corresponding proportion of high tides that are above, or low tides that are below.

The heights of high and low tides are governed by Moon's phase and its position on its elliptical orbit around Earth. At New and Full Moon, Moon and Sun are pulling together on Earth's waters, whereas at First and Third Quarters, they are pulling in opposing directions. Perigee is the closest Moon gets to Earth

each month on its elliptic orbit. Apogee is when it is furthest away. Thus, the pull on Earth's waters is greater in lunar perigee than in lunar apogee. Every 7 months, lunar perigee coincides with a Full or New Moon. In this situation both Sun and Moon are exerting maximum force on Earth's waters and the tidal range is its largest. These are sometimes called "king tides", but a more technical term is perigean spring tides. HAT (highest astronomical tide) is defined in at least two ways: (i) it is the highest tide in a tidal epoch (i.e., 18.6 years); or (ii) it is the sum of the amplitudes of all the tidal constituents. In the old days, when tide forecasting was a significant computing effort, definition (ii) was used, but these days with larger computing power, definition (i) is used. The tables contain a number of useful quantities:

1. Tide heights oscillate between 0.008 and 2.212 m above WCD.
2. MHWS is an important planning level, being the boundary of KDC's domain and the start of DOC's domain. At Kapiti Island, it is 1.923 m above WCD and that level is exceeded by 19.7% of high tides.
3. Some 60% of high tides are above Mean High Water and 60% of low tides are below Mean High Water.
4. Mean High Water Springs and Mean Low Water Springs occur every fortnight just after Full and New Moon.
5. Mean High Water Neaps and Mean Low Water Neaps occur every fortnight just after First and Last Quarter.
6. Mean High Water Perigean Springs and Mean Low Water Perigean Springs, sometimes called "king tides", occur every 207 days when a Full or New Moon coincides with lunar perigee.
7. Mean High Water Apogean Neaps and Mean Low Water Apogean Neaps occur every 207 days when First or Last Quarter coincides with lunar apogee.

Table 6.2 Significant tidal constituents (SNR > 10) at Kapiti Island from annual analyses of 9 years of record from July 1997 to July 2006.

Tidal Con.	Speed °/h	SNR	Amplitude m	Phase ° NZST
O_1	13.94304	54	0.018	28.1
K_1	15.04107	66	0.021	191.3
$2N_2$	27.89535	51	0.016	266.7
μ_2	27.96821	61	0.017	291.4
N_2	28.43973	1540	0.084	274.6
ν_2	28.51258	54	0.015	267.3
H_1	28.94304	16	0.008	158.5
M_2	28.98410	63960	0.552	280.6
λ_2	29.45563	17	0.008	275.8
L_2	29.52848	141	0.023	293.2
T_2	29.95893	85	0.020	343.3
S_2	30.00000	15014	0.261	336.6
K_2	30.08214	1419	0.073	332.1
M_3	43.47616	45	0.021	181.9
SO_3	43.94304	14	0.012	89.9
MK_3	44.02517	15	0.011	127.7
SP_3	44.95893	19	0.014	130.5
S_3	45.00000	32	0.019	328.1
SK_3	45.04107	46	0.021	135.4
MN_4	57.42383	14	0.006	148.7
M_4	57.96821	156	0.023	200.0
MS_4	58.98410	30	0.010	253.6
$2MN_6$	86.40794	12	0.003	82.5
M_6	86.95231	33	0.005	111.7
$2MS_6$	87.96821	12	0.003	134.0

Table 6.3 High tide parameters

High Tide Parameter	Acronym	Level m above WCD	% of high tides above
Highest Astronomical Tide	HAT	2.212	0.0
Mean High Water Perigean Springs	MHWPS	2.007	7.9
Mean High Water Springs	MHWS	1.923	19.7
Mean High Water	MHW	1.662	59.8
Mean High Water Neaps	MHWN	1.400	93.4
Mean High Water Apogean Neaps	MHWAN	1.317	98.8
Mean Level of the Sea	MLOS	1.110	100.0

Table 6.4 Low tide parameters

Low Tide Parameter	Acronym	Level m above WCD	% of low tides below
Mean Level of the Sea	MLOS	1.110	100.0
Mean Low Water Apogean Neaps	MLWAN	0.903	98.8
Mean Low Water Neaps	MLWN	0.820	93.4
Mean Low Water	MLW	0.558	59.8
Mean Low Water Springs	MLWS	0.297	19.7
Mean Low Water Perigean Springs	MLWPS	0.213	7.9
Lowest Astronomical Tide	LAT	0.008	0.0

6.3 Storm Surge

The statistical moments and distribution of storm surge and inverted barometer are presented in Table 6.5. The mean is not shown because it is zero by definition for storm surge and inverted barometer calculated in the way described in Section 4. The standard deviation of storm surge is substantially greater than inverted barometer, but the skewness and kurtosis are similar. The low values of kurtosis indicate there are no large departures (spikes), but the slightly positive values for skewness imply that the crests are higher than the troughs are deep. This is borne out by the distributions which show that the 97.5% and maximum values are larger than the 2.5% and minimum values. If the signals were Gaussian, the skewness and kurtosis would be zero (they are close to that) and the 2.5% and 97.5% values would correspond to ± 1.96 standard deviations.

Thus, storm surge is typically between ± 0.16 m for 95% of the time. Compared with the tide, which varies between ± 1 m about MLOS for 95% of the time, storm surge seems irrelevant. However, unlike the tide, storm surge is episodic and at Kapiti Island it reaches up to 0.373 m above MLOS from time to time.

Indeed, for the 9 years of record, there were 59 events when storm surge exceeded 0.2 m, 17 events when it exceeded 0.25 m and 5 events when it exceeded 0.3 m. These 5 largest events are listed in Table 6.6 and plotted in Figure 6.2. The weather maps for Events 4 and 5 are presented in Figures 6.3 and 6.4. From the weather maps, we see that for both events, the weather situation was basically the same, namely: a trough of low pressure formed in the Tasman Sea and deepened as it drifted eastwards across central New Zealand, accompanied by strong northerly winds. In the Southern Hemisphere, winds blowing with the land on their left cause set-up (positive storm surge), while winds blowing with the land on their right cause set-down (negative storm surge). Thus, on the Kapiti coast, northerly winds increase storm surge and southerly winds reduce it.

Table 6.5 Statistical moments and distributions of storm surge and inverted barometer, where the heights are relative to MLOS.

Parameter	Storm Surge	Inverted Barometer
Std Devn m	0.081	0.068
Skewness	0.264	0.334
Kurtosis	0.338	0.247
Min m	-0.308	-0.195
2.5% m	-0.149	-0.125
50% m	-0.004	-0.004
97.5% m	0.171	0.148
Max m	0.373	0.304

Table 6.6 Details of storm surge events in the measured data that exceeded 0.3 m in height

Event	Time of occurrence	Highest level (m)	Time (h) above 0.3 m
1	02-Jul-1998 04:00	0.330	8
2	23-May-2002 15:00	0.357	21
3	19-Sep-2002 23:00	0.323	12
4	15-Nov-2004 07:00	0.328	12
5	12-Jun-2006 11:00	0.373	23

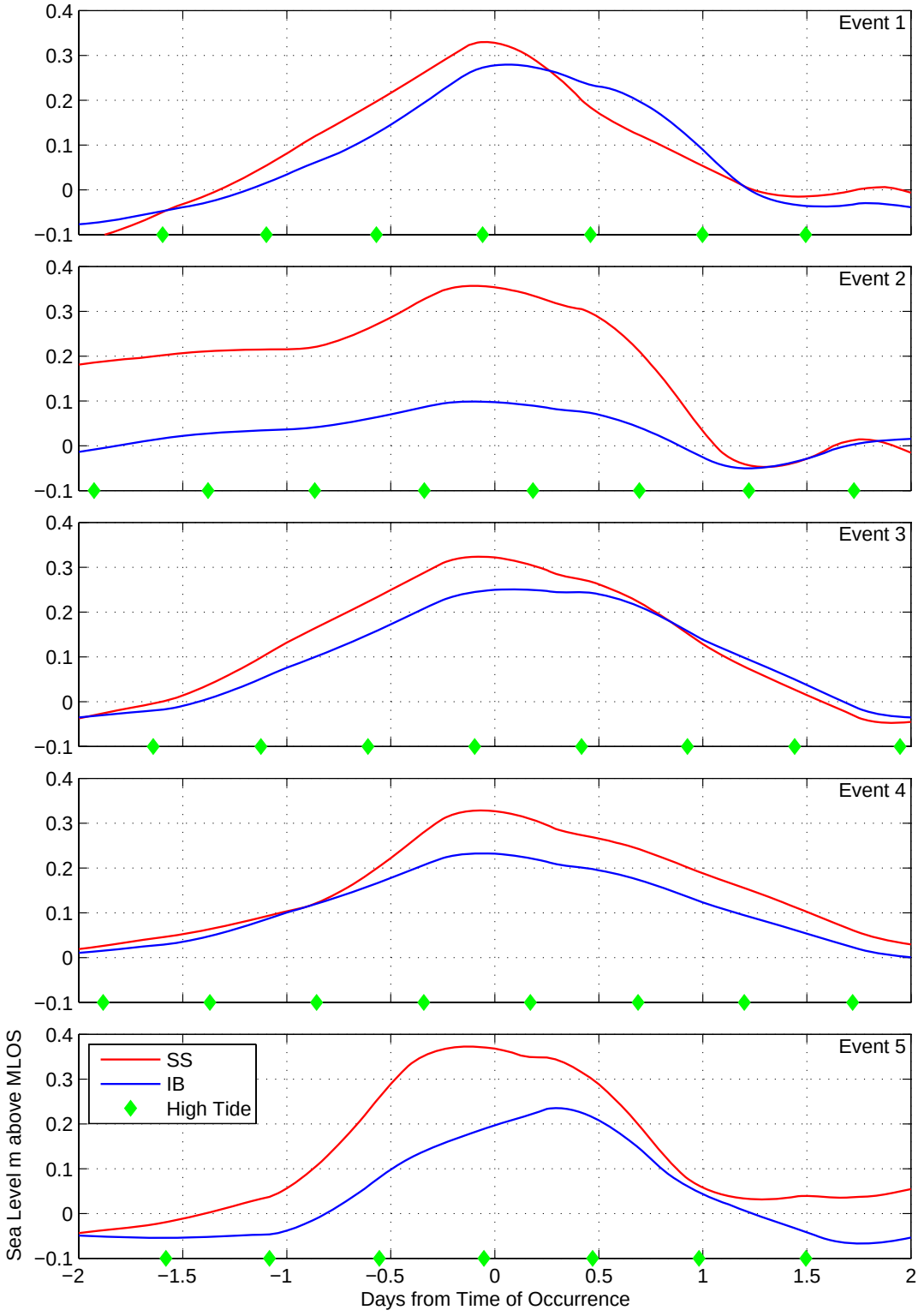

Figure 6.2 Storm surge events larger than 0.3 m (see Table 6.6 for details).

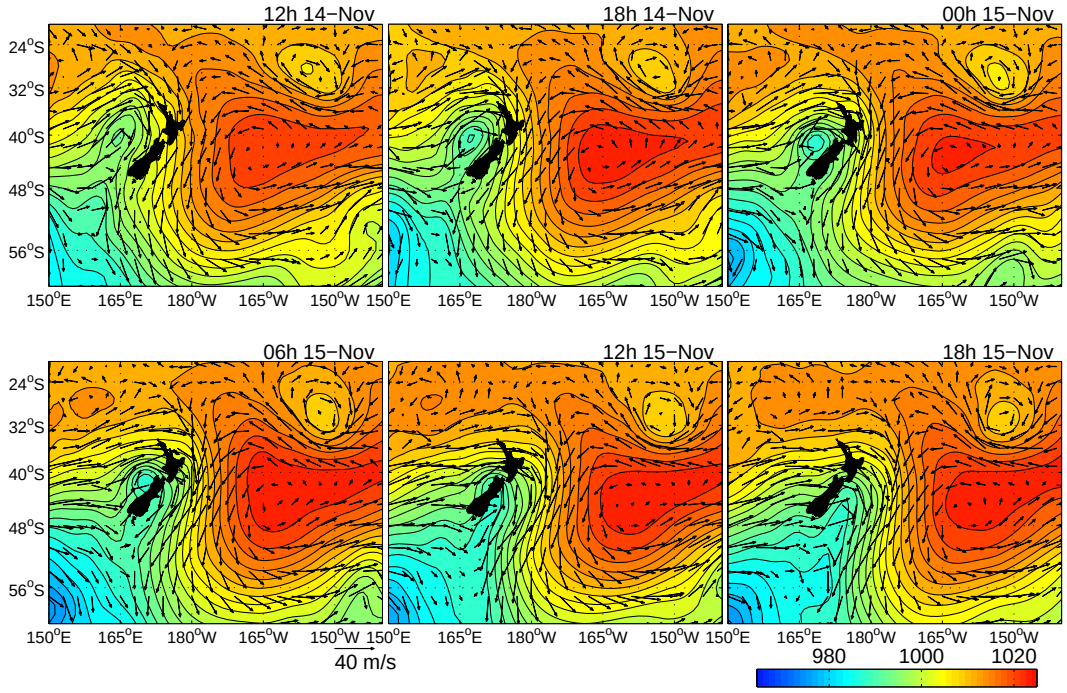

Figure 6.3 Weather maps for storm surge Event 4.

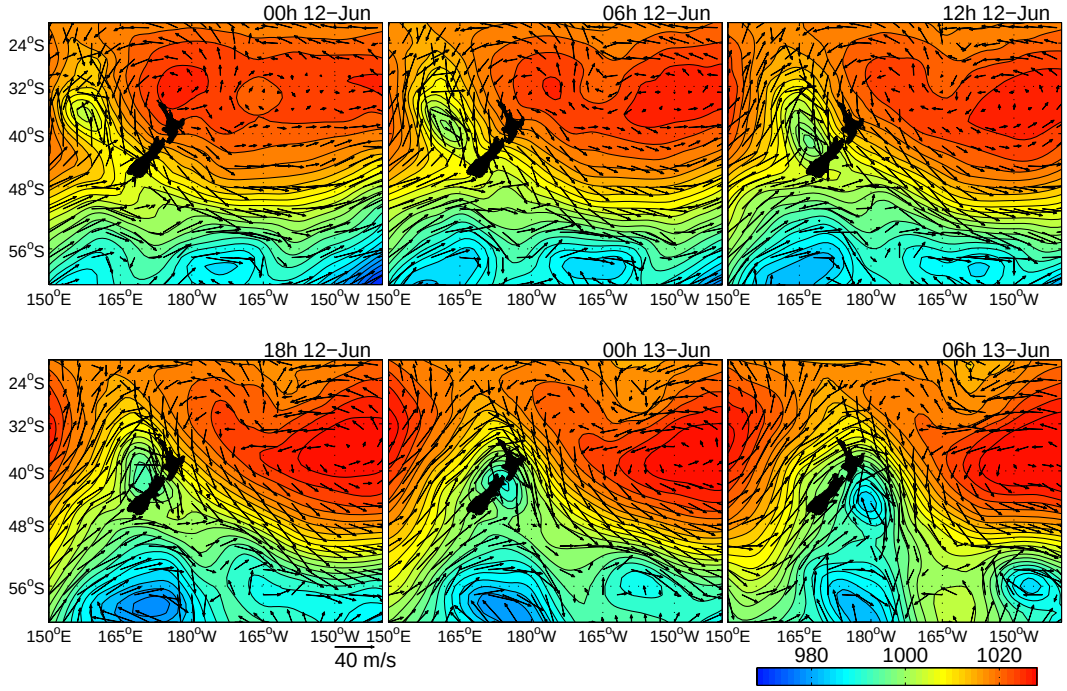

Figure 6.4 Weather maps for storm surge Event 5.

6.3.1 Storm Tide

Figure 6.2 showing the 5 largest storm surge events also shows the time of high tides (green diamonds) and it can be seen that storm surge generally has such a broad crest that at least one high tide occurs when it is at its peak or close to it. Thus, the issue of whether peak storm surge combines with a high tide is not too important: it almost certainly will. What is more important is whether the storm surge occurs at a time when the tidal range is large. For example, if a storm surge of 0.3 m in height occurs at a time of apogean neap tides when the high tide height is 1.317 m above WCD (Table 6.3), sea level will reach 1.317 + 0.3 = 1.617 m above WCD, which is less than mean high water and therefore irrelevant in terms of coastal flooding. However, if the same storm surge occurred at perigean spring tides, sea level would reach 2.3 m above WCD, which is higher than Highest Astronomical Tide and could well cause coastal flooding.

The Revised Joint Probability Method (RJPM) of Tawn & Vassie (1991) is designed to estimate the probability of occurrence for such an event. Table 6.7 is the result of passing 9 years of measured water level data from Kapiti Island through the RJPM. AEP is the inverse of the return period, thus an AEP of 0.01 is equivalent to the 100-year return period. The table shows that for the example considered above of a 0.3 m storm surge occurring during a perigean spring tide and causing a peak sea level of 2.3 m is just below a 10-year return period event.

Also shown in Table 6.7 are the results of using the EST procedure described in Section 4.3.5. For the higher return periods, these results are close to those obtained by RJPM. However, for the results less than 1-year RP, the procedure for EST described in 4.3.5 had to be modified. Instead of using storm surge events, random storm surge heights were combined with random high tides, both drawn from the empirical CDFs. This resulted in higher storm tide heights than using storm surge events. The reason is that storm surge is relatively small compared to high tide heights, so the procedure of using storm surge events to determine the annual maximum storm tide gives a smaller maximum than using

the tide itself. This reflects a difference between conditions in the UK (where RJPM was developed) where storm surge of a metre or two occurs annually, and NZ where storm surge never goes above half a metre. The column headed EST Mod in Table 6.7 shows the result of using high tide heights to determine the maximum storm tide each year. Generally, the storm tide heights are 10 cm higher using this method, and these are the preferred heights for design.

The three rightmost columns in Table 6.7 show the individual exceedances for high tide heights, storm surge, and inverted barometer, drawn from their empirical CDFs. Notice that for tide there is a maximum that is reached after 20 years. This is the HAT (highest astronomical tide) of Table 6.3, being the highest high tide that ever occurs. The storm surge CDF for RPs less than 1-year is based on the 12-hour mean storm surge and inverted barometer, whereas the CDF for 1-year and greater RPs is based on storm surge and inverted barometer events above a threshold of 0.2 m above MLOS. In using these individual exceedances, care needs to be taken in interpreting the datum. Both tide and storm surge (and inverted barometer) are m above WCD, so they cannot be added together without first reducing one of them to MLOS datum by subtracting 1.11 m.

Table 6.7 Annual exceedance probability (AEP), return period (RP) and storm tide (m above WCD) calculated by various methods (see text for details).

AEP	RP	RJPM	EST	EST Mod	Tide	SS	IB
N/A	1/12	N/A	2.16	2.16	2.10	1.30	**1.27**
N/A	3/12	N/A	2.22	2.22	2.14	1.35	**1.31**
N/A	6/12	N/A	2.25	2.25	2.16	1.37	**1.33**
1	1	N/A	2.18	2.28	2.17	1.48	**1.29**
0.50	2	N/A	2.25	2.33	2.18	1.50	**1.31**
0.20	5	2.28	2.30	2.40	2.19	1.52	**1.42**
0.10	10	2.31	2.33	2.44	2.20	1.54	**1.44**
0.05	20	2.34	2.36	2.47	2.20	1.55	**1.45**
0.02	50	2.37	2.39	2.51	2.21	1.57	**1.47**
0.01	100	2.40	2.41	2.53	2.21	1.59	**1.49**
0.005	200	2.43	2.43	2.55	2.21	1.61	**1.50**
0.002	**500**	**2.46**	**2.45**	**2.56**	**2.21**	**1.63**	**1.51**

6.3.2 Storm Surge vs Inverted Barometer

The results of the analysis of inverted barometer against storm surge are presented in Table 6.8. The inverted barometer and storm surge records were split into their wavelet details, and then a regression analysis was carried out on each pair of details, identifying the barometric factor (BF), which is the slope of the regression line. The regression was optimised to find the time lag that gave the largest coefficient of determination, r^2.

Points arising from the table are:

- The lag is positive in all cases, indicating that storm surge **precedes** inverted barometer (this can be seen in Figure 6.2);
- The barometric factor is greater than unity for all but Detail 8, indicating that inverted barometer is amplified to obtain storm surge (also shown in Figure 6.2);
- The coefficient of determination, r^2, indicates the proportion of the variance of storm surge that is explained by inverted barometer, and we see that it is between 69 and 81%.
- The variance indicates the energy in each detail.

The finding that storm surge precedes inverted barometer and the barometric factor is greater than unity agrees with the findings of Goring (1995), which showed this is generally true of west coast sites, though not of east coast sites.

Table 6.8 Results of regression analysis between inverted barometer and storm surge, optimised on time lag.

Component	Timescale	BF	Lag	r^2	Variance cm^2	
	h		h		IB	SS
Detail 5	48	1.324	0.2	0.688	1.8	4.5
Detail 6	96	1.067	0.5	0.761	8.3	12.4
Detail 7	192	1.076	1.5	0.812	17.4	24.8
Detail 8	384	0.947	2.4	0.706	17.9	22.7
All	48-384	1.037	3.0	0.763	46.9	66.2

6.3.3 Inverted Barometer as Surrogate Storm Surge

The digital atmospheric pressure record in New Zealand extends back to 1961 for 17 airports (including Paraparaumu Aerodrome), and as such is much longer than the storm surge record, most of which dates from the mid-90s. Hence, if we could use inverted barometer as surrogate storm surge, we could extend the statistics for storm surge from less than a decade to several decades.

To investigate the efficacy of this, the barometric factor and lag in Table 6.8 were used to transform inverted barometer wavelet details into surrogate storm surge, and then the record was combined with tide and processed using the RJPM. The results are presented in Table 6.9, along with the results of using the 25-year Paraparaumu Aerodrome record, and for comparison the storm surge data from Table 6.7. The table shows that at low return periods, there is some disagreement among the records, but at the high end, the three sources of data produce the same result within a cm.

Table 6.9 Annual exceedance probability (AEP) from the RJPM for: 9 years of IB from Kapiti Island; 25 years of IB from Paraparaumu Aerodrome; and the Kapiti Island sea level record. Levels are m above WCD.

AEP	Return period (yrs)	9-year IB (m)	25-year IB (m)	Storm Tide (m)
0.20	5	2.29	2.30	2.28
0.10	10	2.31	2.32	2.31
0.05	20	2.34	2.34	2.34
0.02	50	2.37	2.38	2.37
0.01	100	2.39	2.40	2.40

6.4 MLOS

The MLOS at Kapiti for the 9 years of record is presented in Figure 6.5. MLOS is calculated by low-pass filtering the residual to remove all oscillations with timescales less than 384 h, then taking monthly means. The upper plot shows the mean annual levels. Note that for 2000, MLOS is 1.11 m, which corresponds to its value at Wellington for this year (see Section 4.3.4 for the explanation). It appears from this figure that in the early years, there was an upward drift in the record, but since 2000 this drift has been arrested and there has been little

variation since. An upward drift in a record corresponds to a fall in the position of the recorder and this could have been caused by the piles of the boatshed slowly sinking before the boatshed was restored in 1999. The mean shown in the plot is the mean over the entire 9 years of record, but if we take the mean of just the years since 2000, it is 1.104 m above WCD. Putting a regression line through the data since 2000 gives a slope of -0.0018 m/y, i.e., sea level has **fallen** at a rate of 1.8 mm/y since 2000, c.f. the average rise of 1.3 mm/y for Auckland over the 20th century (Bell *et al* 2000). As Bell *et al* (2000) explain, MLOS is very sensitive to the effects of El Niño/Southern Oscillation and the Interdecadal Pacific Oscillation, so such falls in MLOS are to be expected in the short term.

The lower plot shows the monthly variation in MLOS, calculated by averaging the levels for each month. It indicates that on average there is a weak annual cycle, with sea levels peaking in May and falling to their lowest level in September, though the year-to-year variation is much larger than the apparent annual cycle. If we exclude the data from before 2000, and assume that MLOS is constant at 1.11 m above WCD, the 95% confidence interval is ± 0.072 m. In other words, there is a 95% probability in any month that the MLOS will lie in the range between 1.038 and 1.182 m above WCD. In practice, this means that 0.072 m should be added for MLOS to estimates of storm surge + tide to obtain design levels.

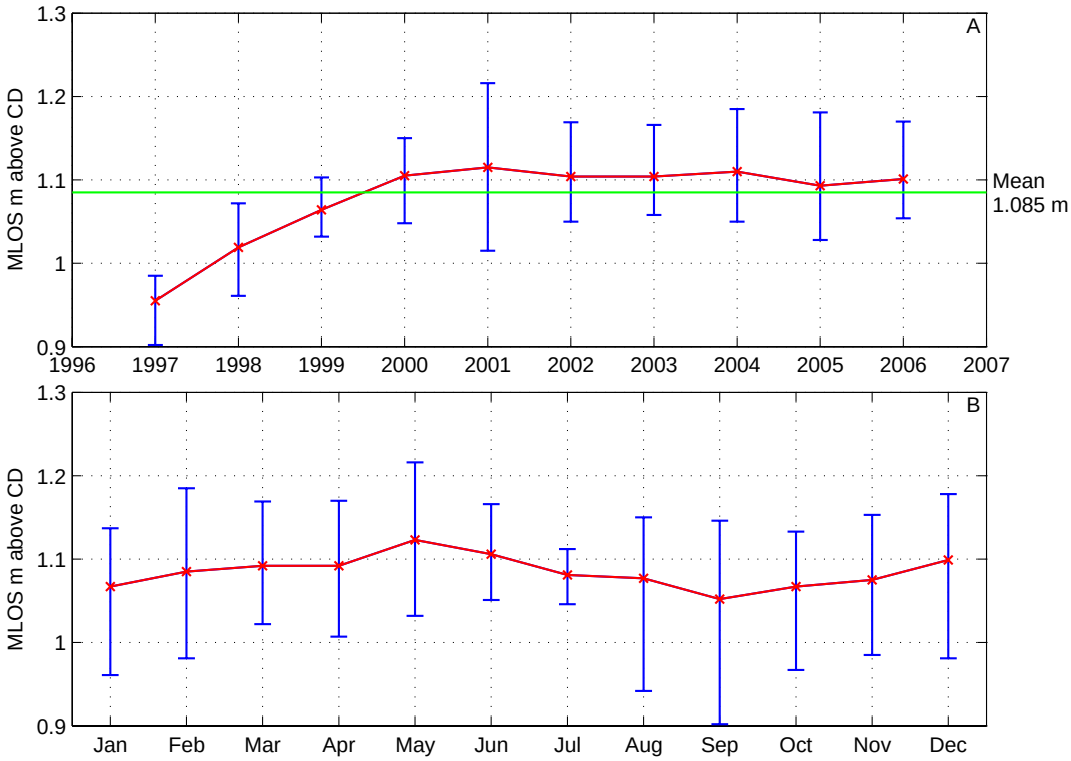

Figure 6.5 Mean level of the sea (MLOS) showing A. the variability in annual means and B. the variability in monthly means.

6.5 Discussion of the water level results

Here, the results of the analysis of the Kapiti Island data are expanded to the mainland coast. Without corroborative evidence, this section is somewhat speculative, but it is the best estimate that is available at present.

Both storm surge and MLOS are large scale phenomenon. We would not expect either to vary spatially along the mainland coast of the Kapiti district. There may be an argument that the sea-level recorder is on the lee side of Kapiti Island and therefore it is sheltered from the setup caused by onshore winds. However, from the analysis of storm surge at various places around New Zealand (Goring, *pers obs*), setup is typically less important. The reason is that New Zealand's weather is unlike the weather at other places where there is large storm surge (like the Bay of Bengal or the North Sea). In those places, depressions sit for days, or even weeks, piling water up on windward shorelines. However, in New Zealand, our depressions travel rapidly across our region and there is not

enough time for the ocean to respond before counteracting winds in the wake of the depression arrive. The weather maps in Figures 6.3 and 6.4 show this quite clearly.

The tide is a different matter altogether, however. Walters *et al* (2001) show that in Cook Strait there is an amphidrome (where the tidal amplitude goes to zero) in the semidiurnal lunar, M_2, tide. The lines of phase radiate out from the amphidrome like spokes in a wheel and the gradient in amplitude is very large. The tides on the mainland coast of the Kapiti district are affected by this to the extent that M_2 has an amplitude of 0.475 m at Paekakariki and 0.678 m at Otaki Beach, 32 km away.

Table 6.10 shows how the tidal parameters vary along the coast for the off shore sites from Figure 5.2, based on the NIWA tide model. The last two lines in the table compare the parameters from the model and their actual values at the sea-level station on Kapiti Island. The comparison of HATs is excellent and gives confidence in the validity of the model. There is a general reduction in HAT from north to south.

Table 6.10 High tide parameters (m above MLOS) for offshore sites along the Kapiti coast and for Kapiti Island (model and actual). See Figure 5.2 and Table 5.1 for the locations.

Site	HAT	MHWPS	MHWS	MHW	MHWN	MHWAN
kpto1	1.268	1.117	0.994	0.688	0.383	0.260
kpto2	1.246	1.097	0.976	0.674	0.372	0.252
kpto3	1.222	1.074	0.957	0.659	0.360	0.243
kpto4	1.201	1.054	0.940	0.644	0.349	0.234
kpto5	1.177	1.032	0.921	0.629	0.337	0.225
kpto6	1.153	1.010	0.902	0.613	0.325	0.217
kpto7	1.130	0.989	0.884	0.599	0.315	0.209
kpto8	1.098	0.961	0.860	0.580	0.301	0.200
kpto9	1.059	0.926	0.831	0.557	0.284	0.188
kpto10	1.018	0.889	0.799	0.533	0.266	0.176
kpto11	0.997	0.871	0.784	0.520	0.257	0.169
kpto12	0.981	0.856	0.770	0.509	0.248	0.163
kpto13	0.961	0.837	0.754	0.496	0.238	0.156
kpto14	0.944	0.822	0.741	0.486	0.230	0.150
kpto15	0.919	0.799	0.722	0.470	0.219	0.141
kpto16	0.901	0.783	0.708	0.459	0.210	0.135
Kapiti (model)	1.103	0.968	0.867	0.587	0.307	0.206
Kapiti (actual)	1.102	0.897	0.813	0.552	0.290	0.207

6.6 Combined Extreme Sea Levels and Waves

Coastal inundation from waves would be exacerbated if sea levels were high. Waves are generated by storms, which also generate storm surge. What is the likelihood of large wave events coinciding with high sea levels? Ramsay & Stephens (2006) have reported finding correlation between these events in a study in Wellington Harbour.

A comparison was made of storm surge events above a threshold of 0.2 m (above MLOS at Kapiti Island) and wave events with heights above 2.5 m at Sites kpto03 and kpto16 (Figure 5.2) for the 9 years of coincident record. The result was that for all the 24 events that coincided within a day, the peak wave height preceded the peak storm surge by at least 6 hours. Typical results are shown in Figure 6.6 and 6.7, which were the largest wave event and the largest storm surge event of the 9 years respectively. Figure 6.6 shows that the peak of the wave event occurred when storm surge was only 0.15 m above MLOS and

that the waves had died away to below 2.5 m at the peak storm surge. Figure 6.7 shows the only event in the 24 where there appears to be significant correlation between waves and storm surge. Thus, in contrast to the findings of Ramsay & Stephens (2006) that for Wellington Harbour waves and sea levels are to some extent dependent, for the Kapiti Coast, storm surge (the stochastic part of sea level) and waves are essentially independent. The reason for the difference is probably related to the vastly different geographical aspects of the two sites: one an open coast exposed to the west, and the other in a harbour which is open to the south.

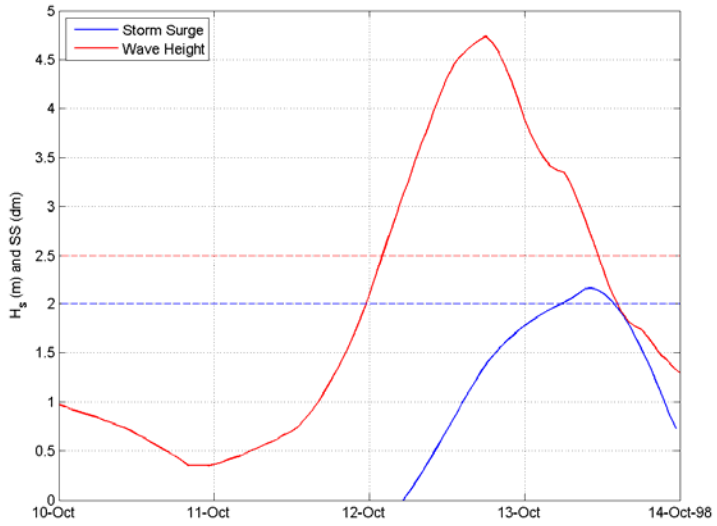

Figure 6.6 **Comparison of the largest wave event and the storm surge at the time, where the dashed lines indicate the thresholds (2.5 m for waves and 2.0 dm for storm surge).**

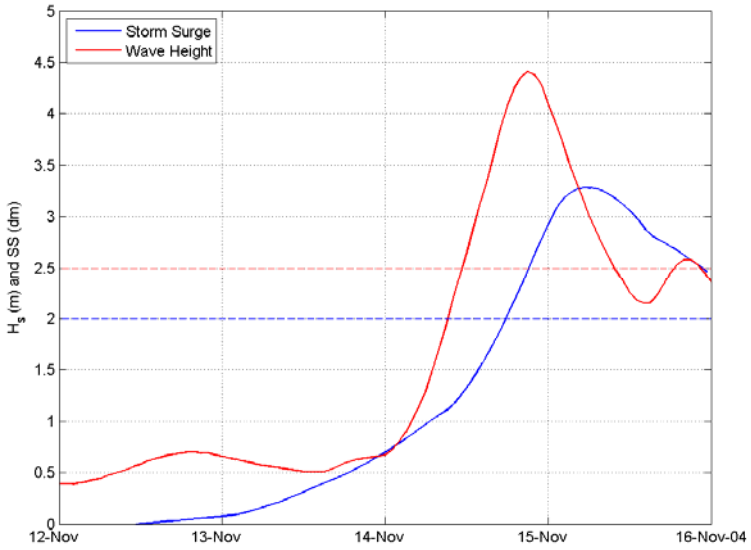

Figure 6.7 Comparison of the largest storm surge event and the waves at the time, where the dashed lines indicate the thresholds (2.5 m for waves and 2.0 dm for storm surge).

Using the Monte Carlo methods described in Section 4.3.5, the joint probability of wave events and sea level events were calculated for a range of return periods, as shown in Tables 6.11a and b for site kpto03 and kpto16 respectively. Each table has two sets of results, one giving the maximum wave height and the associated maximum sea level, and the other giving maximum sea level and the associated wave height. The first point to note is that when we consider maximum wave height, sea levels are all the same; and when we consider maximum sea level, the wave heights are all the same. For maximum wave height, this occurs because only 18 wave events over the threshold occur every year, whereas there are 706 high tides in the year. Therefore, the probability that a wave event will occur on one of the few large high tides is low, and the median high tide (Table 6.3) emerges from the analysis.

The second point is that compared to the wave return periods for kpto03 and kpto16 in Table 5.2, the wave heights calculated using empirical CDFs are somewhat less for larger return periods. The difference arises from different ways of extrapolating beyond the 9 years of data. The data in Table 5.2 were derived from a theoretical distribution whereas those in Table 6.11 were derived

from the shape of the empirical CDF. Which of these is more appropriate is a moot point. However, in practice, the return periods from Table 5.2 should be used in design using only waves, whereas those in Tables 6.12 should be used in design where both waves and sea levels are considered. Sites kpto03 and kpto16 are at the northern and southern ends of the coastal region. For sites between these, the data can be interpolated.

Table 6.11 Joint probability of wave events above 2.5 m and sea level events (in m above WCD) for kpto03.

Return Period	Max^{m} Wave Height		Max^{m} Sea Level	
	Wave Height	Sea Level	Sea Level	Wave Height
1/12	3.44	1.71	1.88	3.07
3/12	3.76	1.72	1.97	3.07
6/12	4.11	1.73	2.06	3.06
1	4.20	1.74	2.08	3.06
2	4.46	1.73	2.13	3.09
5	4.71	1.72	2.19	3.07
10	4.81	1.73	2.22	3.11
20	4.85	1.72	2.25	3.05
50	4.88	1.73	2.29	3.08
100	4.89	1.72	2.31	3.08
200	4.90	1.72	2.34	3.06
500	4.90	1.73	2.37	3.00

Table 6.12 Joint probability of wave events above 2.5 m and sea level events (in m above WCD) for kpto16.

Return Period	Max^{m} Wave Height		Max^{m} Sea Level	
	Wave Height	Sea Level	Sea Level	Wave Height
1/12	3.36	1.71	1.87	2.98
3/12	3.63	1.71	1.97	3.00
6/12	3.93	1.71	2.06	2.98
1	3.95	1.71	2.07	2.98
2	4.21	1.72	2.12	2.97
5	4.46	1.72	2.17	2.98
10	4.56	1.71	2.21	3.01
20	4.60	1.70	2.24	3.01
50	4.62	1.71	2.28	2.96
100	4.63	1.70	2.31	3.01
200	4.63	1.68	2.34	3.00
500	4.63	1.73	2.39	3.03

7 SUMMARY

7.1 Waves

A high-resolution, nested, numerical hindcast of the wave climate along the Kapiti Coast has been undertaken. The hindcast has produced hourly directional wave spectra for 16 discrete locations along the coast, beyond the wave breaker zone. The hindcast duration is from July 1997 – July 2006.

The wave data have been analysed to characterise the ambient wave conditions (annual and monthly) as well as the typical conditions in storm events. The wave climate is characterised by:

- Dominant incident waves from the NW octant.
- The wave climate immediately north of Kapiti Island is slightly more energetic than to the south of the Island.
- There is a wave energy shadow directly behind Kapiti Island (~0.7 reduction in the mean wave height).
- In storm events, the peak spectral wave periods are 7.5 – 9 s.

The significant wave height extrema at 1, 10, 50 and 100-year return periods have been estimated from the hindcast time-series. The 100-year Hs values are 5.50 – 5.95 m away from the shadowing effect of Kapiti Island, reducing to 3.16 m in the direct lee of the Island.

7.2 Water levels

Analysis of 9 years of sea-level and atmospheric pressure data from Kapiti Island, along with 25 years of atmospheric pressure data from Paraparaumu Aerodrome, and weather maps has resulted in the following findings:

- The tide is semidurnal, with a strong fortnightly spring/neap effect. The diurnal tides are very small.
- The largest storm surge occurs when depressions approach from the Tasman Sea, preceded by strong winds from the north or northwest.

- Storm surge at Kapiti Island is relatively small, with only 5 events exceeding 0.3 m above MLOS in the 9 years of record.
- When storm surge combines with tide (storm tide), the 50-year return period sea level is 2.37 m above Wellington Chart Datum (WCD), and the 100-year return period sea level is 2.40 m above WCD. These values were confirmed using 25 years of inverted barometer from Paraparaumu Aerodrome as a surrogate for storm surge.
- Mean level of the sea (MLOS) has fallen by 1.8 mm/y since 2000. There is a weak seasonal component to MLOS, with the peak in May and the trough in September. The 95% confidence interval for month-to-month variation in MLOS is ± 0.072 m.
- The tide varies by 0.32 m in HAT along the Kapiti coast, with the maximum at Otaki and the minimum at Paekakariki. There is a slight rise in tide height at Paraparaumu Beach.

7.3 The coincidence of storm waves and elevated water levels

Wave events generally precede storm surge by 6 hours or more on the Kapiti coast. Thus, since wave events have durations of only a few hours, peak storm surge does not usually coincide with large waves. Simulations found that a sea level of 1.72 m above WCD occurs on average for wave events of all return periods.

REFERENCES

Bell, R.G.; Goring, D. G.; de Lange, W. P. 2000: Sea-level changes and storm surges in the context of climate change. IPENZ Trans., 27:1, 1-10.

Daubechies, I. 1988: Orthonormal bases of compactly supported wavelets. Comm. In Pure and Applied Mathematics, 41: 909-996.

Flather, R.A. (1976) A tidal model of the northwest European continental shelf. Memoires de la Societe Royale des Sciences de Liege 6 (10), 141-164

Goda, Y. (1988). On the methodology of selecting the design wave height. Proc. 21st Coastal Engineering Conf., ASCE, Spain, pp 899-913.

Goring, D. G. 1995: Short-term variations in sea level (2 – 15 days) in the New Zealand region. NZ Journal of Marine and Freshwater Research, 29: 69-82.

Goring, D. G.; Bell, R. G. 1996: Distilling something from patchy tide-gauge records: the New Zealand experience. Special Issue of Marine Geodesy on Sea-Level Networks and Applications, 19: 63-76.

Goring, D. G.; Nikora, V. I. 2002: Despiking acoustic Doppler velocimeter data. ASCE Journal of Hydraulic Engineering, 128(1): 117-126.

Holthuijsen, L.H., Booij, N., Ris, R.C., Haagsma, I.J.G., Kieftenburg, A.T.M.M., Kriezi, E.E., Zijlema, M. and van der Westhuysen, A.J. (2004) SWAN Cycle III version 40.31 User manual. Available: http://fluidmechanics.tudelft.nl/swan/index.htm

Hubbard, B. B. 1996: The World According to Wavelets: the story of a mathematical technique in the making. A. K. Peters, 264pp.

Leenknecht, D., Szuwalski, A. & Sherlock, A. (1991) AUTOMATED COASTAL ENGINEERING SYSTEM (Version 1.05), Extremal Significant Wave Height Analysis - Ch.1.3, CERC-Vicksburg, ACES Technical Reference 159 p, USA Department of the Navy.

Marchesiello, P., Mc Williams, J.C. and Shchepetkin, A. (2001) Open boundary conditions for the long-term integration of regional oceanic models. Ocean Modelling, 3, 1-20

Mathiesen, M., Goda, Y., Hawkes, P., Mansard, E., Martin, M., Peltier, E., Thompson, E & Vedder, G., (1994). Recommended practice for extreme wave analysis. Journal of Hydraulic Research, 32 (6), 803-814.

Mellor, G.L. (2004) Users guide for "A three-dimensional, primitive equation, numerical ocean model". Princeton University, Princeton, NJ. Available from: http://www.aos.princeton.edu/WWPUBLIC/htdocs.pom/

Misiti, M.; Misiti, Y.; Oppenheim, G.; and Poggi, J.-M. 2000: Wavelet Toolbox Users's Guide. The Mathworks Inc.,

Pawlowicz, R.; Beardsley B.; Lentz, S. 2002: Classical tidal harmonic analysis including error

estimates in MATLAB using T_TIDE, Computers and Geosciences 28: 929-937.

Ramsay, D.; Stephens, S. 2006: Double trouble: How often do large waves occur with high water levels? *Coastal News* 32, pp 4:5.

Scheffner, N. W.; Borgman, L. E.; Mark, D. J. 1996: Empirical simulation technique based storm surge frequency analyses. *ASCE Journal of Waterway, Port, Coastal, and Ocean Engineering*, 122(2): 93:101.

Tawn, J. A.; Vassie, J. M. 1991: Recent improvements in the joint probability method for estimating extreme sea levels. In Tidal Hydrodynamics, B. B. Parker (ed). John Wiley & Sons, pp 813:828.

Tolman, H.L. and D. Chalikov, 1996: Source terms in a third-generation wind-wave model. J. Phys. Oceanogr, 26, 2497-2518.

Walters, R. A.; Goring, D. G.; Bell, R. G. 2001: Ocean tide around New Zealand. NZ Journal of Marine and Freshwater Research, 35: 567-579.